HHS Public Access

Author manuscript

Brain Imaging Behav. Author manuscript; available in PMC 2021 June 01.

Published in final edited form as:

Brain Imaging Behav. 2020 June ; 14(3): 696–714. doi:10.1007/s11682-018-0006-y.

Individual variations of the human corticospinal tract and its hand-related motor fibers using diffusion MRI tractography

K. Dalamagkas[1,2,3,4,5,*], **M. Tsintou**[1,2,5,6,*], **Y. Rathi**[2], **L.J. O'Donnell**[2], **O. Pasternak**[2,7], **X. Gong**, **A. Zhu**, **P. Savadjiev**[2,7], **G.M. Papadimitriou**[6], **M. Kubicki**[2,6,7], **E.H. Yeterian**[8], **N. Makris**[2,6,9]

[1.]Surgical Planning Laboratory, Brigham and Women's Hospital, Harvard Medical School, 1249 Boylston, 02215, Boston, MA, USA

[2.]Department of Psychiatry, Psychiatry Neuroimaging Laboratory, Brigham and Women's Hospital, Harvard Medical School, Boston, MA, USA

[3.]Department of Physical Medicine and Rehabilitation, The University of Texas Health Science Center at Houston, Houston, TX, United States

[4.]TIRR Memorial Hermann Research Center, TIRR Memorial Hermann Hospital, Houston, TX, United States

[5.]UCL Division of Surgery & Interventional Science, Center for Nanotechnology & Regenerative Medicine, University College London, London, UK

[6.]Department of Psychiatry and Neurology Services, Center for Neural Systems Investigations, Center for Morphometric Analysis, Athinoula A. Martinos Center for Biomedical Imaging, Massachusetts General Hospital, Harvard Medical School, Boston, MA 02129, USA

[7.]Department of Radiology, Brigham and Women's Hospital, Harvard Medical School, Boston, MA, USA

[8.]Department of Psychology, Colby College, Waterville, ME, 04901, USA

[9.]Department of Anatomy & Neurobiology, Boston University School of Medicine, Boston, MA, USA

Abstract

The corticospinal tract (CST) is one of the most well studied tracts in human neuroanatomy. Its clinical significance can be demonstrated in many notable traumatic conditions and diseases such as stroke, spinal cord injury (SCI) or amyotrophic lateral sclerosis (ALS). With the advent of

Corresponding Author: Nikos Makris, nikos@cma.mgh.harvard.edu, Telephone number: 617-726-5743.

*The authors marked with contributed equally to this work.

[7]Compliance with ethical standards

[7.1]Conflicts of interest

The authors declare that they have no conflict of interest.

[7.2]Ethical approval

For this type of study formal consent is not required.

[7.3]Informed consent

Informed consent was obtained from all individual participants included in the study.

diffusion MRI and tractography the computational representation of the human CST in a 3D model became available. However, the representation of the entire CST and, specifically, the hand motor area has remained elusive. In this paper we propose a novel method, using manually drawn ROIs based on robustly identifiable neuroanatomic structures to delineate the entire CST and isolate its hand motor representation as well as to estimate their variability and generate a database of their volume, length and biophysical parameters. Using 37 healthy human subjects we performed a qualitative and quantitative analysis of the CST and the hand-related motor fiber tracts (HMFTs). Finally, we have created variability heat maps from 37 subjects for both the aforementioned tracts, which could be utilized as a reference for future studies with clinical focus to explore neuropathology in both trauma and disease states.

Keywords

two-tensor tractography; diffusion tensor imaging; corticospinal tract; neural repair; quantification

1 Introduction

Of primary relevance and clinical interest among the fiber pathways in the human brain have been the pathways associated with motor function and, more specifically, the corticospinal tract (CST). Strictly speaking, the CST is the large descending fiber tract that originates in the cerebral cortex and extends longitudinally through the bulbar pyramid. The terms CST and pyramidal tract (PT) are often used interchangeably (e.g., (Mai and Paxinos 2011)), and are used synonymously in the present study. The anatomy of the CST and its correlation with clinical outcomes has been the focus of medical research since the 1600s. Willis (Willis 1664) described and named the pyramids of the medulla in the macrodissected adult human brain and in other large mammals, stating that they resembled great nerves. Mistichelli (1709, cited in (Finger 1994)) described crossing fibers on the ventral surface of the medulla and published an illustration of the pyramidal decussation. However, he maintained that these fibers originated from the dura mater. One year later, Pourfour du Petit (1710, cited in (Finger 1994), and in (Clarke and O'Malley 1996)) gave a description of the fiber architecture of the pyramidal decussation using postmortem human and experimental animal (dogs) material. He provided his own illustrations of the decussating fibers in the pyramids, and noted that the cerebral cortex has a direct role in movement. It was in the 1800s that Gall and Spurzheim (Gall and Spurzheim 1810) associated the PT with motor function and that Cruveilhier (Cruveilhier 1853) correlated its atrophy with contralateral paralysis. Türck ((Türck 1851); 1852, cited in (Clarke and O'Malley 1996)), using secondary degeneration methods, observed both crossed and uncrossed pyramidal tract fibers. Türck believed the pyramidal tract originated in the basal gray matter of the brain and not in cerebral cortex. Thus, he used "pyramidal" to denote the pyramids of the brainstem rather than Betz cells, which had not yet been described. A few years later, the crossed and uncrossed pyramidal fibers were recognized by Bouchard (Bouchard 1866) as parts of the PT. Finally, the uncrossed lateral PT fibers were identified in the macaque by Schäfer (Schäfer 1883) as well as in human pathological material by Pitres (Pitres 1884). In 1877, Flechsig (Flechsig 1877) observed in pathological material that lesions of the motor area of the cerebral cortex result in degeneration of the PT. In 1904, Flechsig (Flechsig 1904) noted that the cortical origin of

the PT, i.e., the CST, appeared to be the middle and upper thirds of the precentral gyrus. Shortly thereafter, Holmes and May (Holmes and May 1909) provided further insight on the cortical architectonic origins of the CST, identifying the source as the giant pyramidal cells of Betz in Brodmann's area 4 (BA 4). Since the early 1900s, qualitative studies have been complemented by quantitative investigations (Campbell 1905; Ford and Hackney 1997; Hille 2001; Lassek and Rasmussen 1939; Parent 1996; Pellegrino et al. 1984; Yagishita et al. 1994) that have produced a detailed understanding of the CST in terms of number of cells and fibers composing this fiber tract in humans.

Experimental studies of the rodent and non-human primate CST have elucidated the anatomy and physiology of the motor system (Barnard and Woolsey 1956; Kuypers 1958; Kuypers 1964; Levin and Beadford 1938; Nyberg-Hansen and Rinvik 1963; Peele 1942; Russell and DeMyer 1961). In particular, based on some of those studies, the present consensus is that the origin of the CST is more restricted in humans compared to non-human primates. In humans the CST is currently thought to originate from BA 4 (primary motor cortex, giving rise to about 60% of the CST fibers), area 6 (supplementary motor area) and part of the parietal lobes (Davidoff 1990). These studies are highly relevant, given their translational potential to humans, especially in the clinical domain of neuroregeneration and repair. Importantly, in order to be able to screen for pathological findings, track clinical progress and detect the regenerative potential of developing therapies, clinicians and researchers need to know the anatomy of the individual subject.

The advent of diffusion magnetic resonance imaging (dMRI) (Basser et al. 1994; Le Bihan et al. 1986) has greatly facilitated the study of neural connections in humans, both ex vivo and, most importantly, in vivo in a non-invasive fashion. Although dMRI is a powerful approach for studying brain connections there are limitations that need to be overcome. Both the diffusion tensor imaging (DTI) and high angular resolution diffusion imaging (HARDI) techniques (Basser et al. 1994; Tuch et al. 2002) have permitted a more valid examination of the most sizeable and best defined fiber tracts in humans (Makris et al. 2005; Schmahmann and Pandya 2006). Thus, pioneering studies using diffusion imaging-based segmentation (Makris et al. 1997; Makris et al. 2005) and tractographic approaches (Lori et al. 2002; Mori et al. 1999) aimed at delineating the corpus callosum (Huang et al. 2005), CST (Stieltjes et al. 2001), optic radiations (Sherbondy et al. 2008) and the major corticocortical association fiber tracts (Makris et al. 1997, p. 199; Mori et al. 1999) in humans. Given the anatomical location of the hand representation in the posterior limb of the internal capsule (IC) (Bertrand et al. 1965; Chronister and Hardy 1997) and its considerable size and well-known anatomy in humans, the CST may be one of the most highly studied fiber pathways in the human brain (Betz 1874; Lassek and Rasmussen 1939; Parent 1996). Several investigations of its physiology (Schäfer 1910), function (Bertrand et al. 1965), clinical significance (Dejerine and Dejerine-Klumpke 1895; Hirayama et al. 1962), and MRI-based characterization (Chen et al. 2016; Ellis et al. 2001; Holodny et al. 2005; Kuo et al. 2017; Lee et al. 2015; Mandelli et al. 2014; Mormina et al. 2015; Pierpaoli et al. 2001; Yagishita et al. 1994) have yielded information indicating the importance of accurately and precisely mapping its different components, and the hand area in particular, given its key clinical significance for motor and sensory functions in humans (Le Gros Clark 1959; Skirven et al. 2011). Several studies have attempted to delineate the hand-related motor fiber tracts

(HMFTs) as part of the CST using a multimodal imaging approach with dMRI tractography and fMRI or utilizing invasive techniques such as intraoperative electrical stimulation (Berman et al. 2004; Bucci et al. 2013; Hamidian et al. 2018; Jeong et al. 2015; Lee et al. 2016; Mandelli et al. 2014; Qazi et al. 2009; Radmanesh et al. 2015; Weiss et al. 2015). Nevertheless, despite the great clinical significance of the hand motor area for a patient's independence in terms of the activities of daily living, the HMFTs have not been explored as part of the CST using solely dMRI tractography in healthy subjects. Therefore, an assessment of the anatomical variability of the CST and HMFTs is critical. It is essential that such studies, in conjunction with future studies focusing on the functional aspect of the motor tracts using fMRI and clinical functional scales, become a bridge between human brain anatomy and function, to allow for more reliable prediction of the neuroregenerative impact of novel therapies on human subjects, utilizing non-invasive imaging tools with objective scales. The CST is affected in several neurological entities, such as stroke and spinal cord injury (SCI) and several neurodegenerative diseases (Ropper et al. 2014). Stroke and SCI alone have a tremendous impact on the general population with huge personal and financial costs to society. Thus, clinical trials involving molecules, cells or even biomaterials, aimed at minimizing or even reversing the impact of CST trauma and creating an appropriate environment for regeneration and repair, are currently underway involving interdisciplinary research. MRI diffusion tensor imaging, and especially tractography, is an excellent tool for the establishment of grounds for a common scale "language" among interdisciplinary teams. dMRI tractography could pave the way for development of an objective scale and could catalyze the discovery of new interventions to benefit a vast population of CST patients.

Currently, there is no single method for tracking the CST for surgical planning with accuracy and reliability. Moreover, beyond treatment purposes, understanding the causal role of the CST for specific neurological conditions is of great importance. Unfortunately, only pathological data from postmortem studies are available for exploration in the human population. Thus, pursuing non-invasive in vivo imaging of the CST using dMRI is an attractive prospect from both clinical and basic research perspectives. Diffusion MRI tractography has been widely used in pre-surgical planning, with the CST being one of the tracts frequently studied due to its importance for voluntary movement (Berman et al. 2004; Bucci et al. 2013; Chen et al. 2016; Kinoshita et al. 2005; Snow et al. 2016).

Given the great clinical importance of the HMFTs within the CST, we designed experiments to test our hypothesis that dMRI tractography can be used to adequately delineate the HMFTs as part of the CST. Any potential functional correlations would be of utmost importance for relating anatomy to neuropathology and clinical status, especially in diseased subjects; however, this is beyond the scope of the present study, which is focused strictly on structural assessment of the aforementioned motor tracts using dMRI tractography and exploration of anatomical variability among healthy subjects. In this study we delineated and quantified the CST as a whole as well as its hand motor representation in 37 healthy human subjects derived from the Human Connectome Project (HCP) DTI datasets. To this end, we applied two-tensor tractography, a higher-order dMRI-based tractographic procedure. Furthermore, we assessed inter-subject topographic variability of the CST and the HMFT in particular in this subject population. To the best of our knowledge, this is the first attempt to

fully delineate the HMFTs as part of the CST using purely dMRI tractography, including determining the variation of the tracts within a healthy population.

2 Methods

2.1 Aims

We used dMRI two-tensor unscented Kalman filter deterministic tractography (UKF deterministic tractography) in 37 healthy human subjects with state-of-the-art data to accomplish four main goals: a) to anatomically delineate the complete CST, b) to isolate the hand-related motor area as a subset of the CST, c) to generate a database of volume, length and biophysical parameters such as fractional anisotropy (FA) (Basser 2004), axial diffusivity (AD) (Song et al. 2003), and radial diffusivity (RD) (Song et al. 2002, 2003) for the CST and for the HMFTs, and d) to quantify the variability of the CST and of the HMFTs within the healthy population using probabilistic variability maps (heat maps).

2.2 Subjects

Thirty-seven healthy adult subjects (mean age=30.88, SD=3.14), 19 male (mean age=30.42, SD=3.37) and 18 female (mean age=31.36, SD=2.89), were used for this analysis from the state-of-the-art WashU Connectome Project led by Washington University (http://www.humanconnectome.org/data/), University of Minnesota and Oxford University (the WU-Minn HCP consortium) and in particular from the HCP 500 Subject Release of 2013. Almost 65% of the tested subjects were 31–35 years old (45.8% of male subjects and 54.2% of female subjects, within that age group). Of the total subjects, 27% were 26–30 years old (60% of male subjects and 40% of female subjects, within that age group) and only 8% were 22–25 years old (66.7% of male subjects and 33.3% of female subjects, within that age group).

2.3 MRI procedures

The data were acquired with the specially configured WU-Minn Skyra Connectome scanner from Siemens using a 32-channel standard Skyra coil. Customized hardware with gradient coil and gradient power amplifiers for research use increased the maximum gradient strength from standard 40 mT/m to 100 mT/m on the WU-Minn 3T scanner. Diffusion datasets were acquired with 1.25 × 1.25 × 1.25 mm^3 voxels, FOV = 210mm, 111 slices, TE = 89.50ms, TR = 5520ms, b-value= 1000, 2000, 3000s/mm^2, 90 directions per b-value and 18 non-diffusion-weighted volumes (Uğurbil et al. 2013). For our analysis we used only the b-value 3000s/mm^2 data given the superiority of these data for detecting more connections in complex tracts such as the CST (Berman et al. 2013; Caiazzo et al. 2018).

2.4 Tractographic Delineation of the CST

This dataset is a subset of the publicly available HCP (http://www.humanconnectome.org/data/). Therefore, it was already processed through the HCP preprocessing pipeline described in the original paper (Glasser et al. 2013). UKF tractography was performed using a multi-tensor tractographic algorithm (Malcolm et al. 2010) and quality control analysis of the tractography followed. Based on prior results, two-tensor UKF tractography (Malcolm et al. 2010) was chosen as a more sensitive method for the delineation of the CST, allowing

fiber tracing in areas known to be heavily affected by crossing fibers and branching (Baumgartner et al. 2012; Chen et al. 2016). In an attempt to increase accuracy, aimed at future clinical applicability of the method, we chose to manually draw certain regions of interest (ROIs) using anatomical landmarks for the CST and hand motor area rather than using automatic methods. We then used the White Matter Query Language (WMQL) (Wassermann et al. 2013) to delineate the fiber tracts passing through all the drawn ROIs and proceeded with the quantification methodology after activating the two tensors and performing quality control analysis once again.

2.4.1 Two-tensor Deterministic Tractography: Manual Segmentation and Inter-rater and Intra-rater Reliability—

After completing quality control for the UKF tractography, the 3D Slicer software package (version 4.4.0, www.slicer.org) via the SlicerDMRI (Fedorov et al. 2012; Norton et al. 2017) project (dmri.slicer.org) was used to create the tensors mask and then sample the ROIs. The CST was delineated using three ROIs, which were manually drawn in 3D Slicer in axial color-coded dMRI sections as shown in detail in Fig. 1. Specifically, the first ROI was in the upper medulla rostral to the inferior olivary nucleus (hereinafter referred to as medulla-ROI); the second ROI was at a mesencephalic level rostral to the substantia nigra and red nucleus (hereinafter referred to as brainstem-ROI); and the third ROI was in the internal capsule (IC) at the anterior commissure (AC) level (hereinafter referred to as capsular-ROI) (Fig. 1). In the medulla- and brainstem-ROIs we selected only voxels with fibers in the vertical dimension (Z-axis), which were color-coded blue. In the capsular-ROI we included all voxels of the IC.

WMQL software (Wassermann et al. 2016) was used for the extraction of fiber bundles based on the manually drawn ROIs so that the fibers passed through all three ROIs. Subsequently, the results were visualized in 3D Slicer for quality control and refined by removing any commissural fibers that were not part of the CST.

The two raters (K.D. and M.T.) received independent training and worked independently during the rating stage to avoid any bias. For the inter-rater reliability process, K.D. processed all 37 WashU subjects and M.T. processed 10 randomly selected WashU subjects independently. The results for the 10 common cases were compared for the two independent raters using Cronbach's Alpha reliability analysis in the SPSS v23 statistical software package (Cronbach 1951).

To assess intra-rater reliability, M.T. processed the previously randomly selected 10 WashU cases for a second time several days after the initial processing, without referring to the previous results. For this process the results for those 10 cases were compared using the SPSS v23 statistical software package. As for the inter-rater reliability, the intra-rater reliability assessment was done by performing Cronbach's Alpha reliability analysis.

2.5 Quantitative Analyses

The tract biophysical characteristics (i.e., tract volume, tract length, FA, RD, AD) were obtained in all 37 healthy human subjects. The diffusion imaging biophysical parameters of FA, AD and RD may relate to fiber tract coherence and integrity (Basser 2004; Song et al.

2002, 2003). We normalized the tract volume results by the whole brain volume for each individual to avoid any inconsistencies due to personal characteristics.

Symmetry indexes (SI) $\left(Symmetry\ Index\ (SI) = \frac{Left - Right}{0.5 * (Left + Right)}\right)$ for left and right tracts (Galaburda et al. 1987) for measures of volume, mean FA, mean AD and mean RD were calculated for each individual, and across subjects. In addition the presence of outliers in the aforementioned measures such as FA, AD, RD and volume was tested using Tukey's range test in the initially delineated CSTs and then in the delineated HMFTs (Tukey 1977).

2.6 Isolation of the HMFTs

Based on the previous work of Yousry et al. (Yousry et al. 1997) who used fMRI to accurately define the hand motor area in structural MRI scans, the hand motor area was defined in the axial plane as a knob-like, broad-based, posterolaterally directed region of the precentral gyrus. This region usually has an inverted omega shape and sometimes a horizontal epsilon shape, with a mean diameter of 1.4 cm. On average it is located about 23 mm from the midline, just posterior to the junction of the superior frontal sulcus with the precentral sulcus and 19 mm from the lateral surface. In the sagittal plane, this knob takes the form of a posteriorly directed hook with a mean depth and height of 17 and 19 mm, respectively. It is located in the sagittal plane of the same section in which the insula can be identified, perpendicular to its posterior end. In neurologically unaffected hemispheres like the ones we used in the present study, the sensitivity of detecting the hand motor area in a structural MRI scan with this method has been shown to be 97–100%, with an accuracy of 97–100% (Yousry et al. 1997).

To isolate the hand motor area, we used 3D Slicer to draw a fourth ROI in the area of the "omega sign" in the axial plane, and the drawing process was completed in the coronal plane (hereinafter referred to as cortical-ROI). In order to ensure as accurate a location as possible for the "omega sign" in the precentral gyrus we used in parallel the FreeSurfer labelmaps created by the process of automatic subcortical segmentation for each subject. By using the slice intersection feature of 3D Slicer the same area was located in the coronal plane. The remaining non-colored area of gyri, defined by the previously drawn colored marks of the axial plane, was filled in with the same color, as illustrated in Fig. 2a. All four ROIs (the previously drawn three ROIs and the new one for the hand area) were merged into one labelmap, which was then used with the WMQL software to extract the fiber bundles emanating from all four ROIs, thereby isolating the HMFTs (Fig. 2b). The isolated HMFTs represented a subset of the initial CST and required no further refinement. We note that using this manual procedure to select the ROIs makes the delineation of the fiber tracts robust with regard to errors in EPI distortions in the brainstem region as reported in Irfanoglu et al. (Irfanoglu et al. 2015).

2.7 Assessment of inter-subject variability of CST and HMFTs

We generated probabilistic maps for the CST and the HMFTs in Montreal Neurological Institute (MNI) 152 standard space, by first registering each subject to an MNI152 template with a resolution of $1mm^3$. Affine transformation was used for the co-registration of our fiber bundles and the baseline b0 brain MRI images. We registered our subjects to MNI

space using non-rigid registration to spatially normalize the tractography files. The purpose was to obtain a heat map of the CST and HMFTs, so that the inter-subject variability could be readily appreciated by visual inspection. The CSTs and the HMFTs were processed with the pipeline described above.

We calculated a fiber tract mask on the MNI152 template for each subject using 3D Slicer software. In this mask a voxel had a value only if a tract traversed it. Finally, we averaged the masks for all our subjects in order to produce the probabilistic heat map for the CST and repeated the same process for the HMFTs.

2.8 Crossing fibers interference analysis of HMFTs

We ran two sets of experiments to determine the effect that crossing fibers at the level of the CST have on our hand motor area findings. The first set of experiments entailed the delineation of the arcuate fascicle (AF) and the superior longitudinal fascicles, i.e., SLF I, SLF II and SLF III, using the WMQL software's automatic fiber extraction method (http://tract-querier.readthedocs.io/en/latest/#) based on previously described definitions of the tracts (Wassermann et al. 2013). The second set of experiments involved the delineation of the corpus callosum (CC) fiber tracts based on a variant of the WMQL-based published methodology (Wassermann et al. 2016) to isolate the 7 subsections of the CC. The quantification and the MNI space co-registration were performed as described in sections 2.5 and 2.7, respectively.

3 Results

3.1 Delineation of the CST and HMFTs

This study delineated the CST using state-of-the-art data, with the combination of a tractographic algorithm and 3 manually drawn ROIs. Fig. 3 illustrates a representative example of a CST delineation using our methodology. Our approach allowed us to delineate the CST without fiber truncations and with a limited effect of crossing fibers interference. Nevertheless, as indicated by Fig. 4, the hand motor area, which is the focus of our study due to its clinical significance, still seems to be affected by technique-related limitations. Fig. 4 is a representative example, demonstrating a significant paucity of fibers of the hand motor area. It should be noted that in our sample of 37 subjects, only one case showed extremely poor CST representation and, therefore, was considered an outlier and was excluded from the HMFT analysis.

Following delineation of the CST, the hand motor area was isolated as described in section 2.6, adding the cortical-ROI in our method. Despite existing limitations, the HMFTs were isolated in 36 of 37 cases. The only case with an absent HMFT was that with the initially poor CST; therefore, this result was not associated with the HMFT-related methodology. As expected from prior experience and our CST results, the hand motor area isolation was much more challenging and the paucity of fibers in that region was evident in some subjects. Moreover, a greater inter-subject variability was noted on the initial visual inspection of the HMFTs. A representative example of our isolated HMFTs is shown in Fig. 5.

3.2 Inter-rater and intra-rater reliability

Cronbach's Alpha values were used to determine inter- and intra-rater reliability for the present technique, which was found to be highly replicable. The most reliable values in our study are for the diffusion parameters (i.e., FA, RD, AD values), with Cronbach's alpha approaching the maximum of 1.00 (0.95 for FA inter- and FA intra-rater reliability; 0.99 for RD inter- and intra-rater reliability; 0.98 for AD inter- and intra-rater reliability). Tract volume was found to be moderately reliable (0.80 for inter-rater and 0.90 for intra-rater reliability) and the number of fibers was found to be less reliable (0.70 for inter-rater and 0.68 for intra-rater reliability); nevertheless, all values were considered to be within an acceptable range. This is in agreement with previous studies (Carlson et al. 2014; Dini et al. 2013) that, even having used a different approach, yielded similar outcomes in exploring the reliability and reproducibility of dMRI tractography analysis parameters for certain tracts.

3.3 Quantitative Analyses

We generated a database of biophysical parameters (i.e., FA, AD, RD) and volume of the CST and the HMFTs (Tables 1 and 2).

The CST had a mean volume of 21.187 cm^3, SD=6.083 (left CST: mean volume=11.081 cm^3, SD=3.760; right CST: mean volume=10.479 cm^3, SD=3.670). After normalizing the tract volumes by dividing by the total brain volume to yield a fraction of the whole brain volume, the CST mean volume fraction was 0.014, SD= 0.004 (left CST: mean volume fraction= 0.007, SD= 0.002; right CST: mean volume fraction= 0.007, SD= 0.003). The mean FA value of the CST was 0.708, SD=0.018 (left CST: mean FA= 0.708, SD=0.018; right CST: mean FA= 0.705, SD=0.022). The coefficient of variation was <10% for all parameters tested, except for the tract volume which was highly variable among the subjects (coefficient of variation approximately 30%). Overall, FA was the most reliable parameter for our study with a coefficient of variation of only about 2.5%. This agrees with other reports noting the same variability trend (Carlson et al. 2014).

Regarding the HMFTs, the mean volume was 2.770 cm^3, SD=1.383 (left HMFTs: mean volume=1.255 cm^3, SD=1.001; right HMFTs: mean volume=1.544 cm^3, SD=0.882). After normalizing the tract volumes by dividing by the total brain volume to yield a fraction of the whole brain volume, the HMFTs' mean volume fraction was 0.002, SD= 0.001 (left HMFTs: mean volume fraction= 0.001, SD= 0.001; right HMFTs: mean volume fraction= 0.001, SD= 0.001). The mean FA value of the HMFTs was 0.673, SD= 0.121 (left HMFTs: mean FA= 0.601, SD= 0.246; right HMFTs: mean FA= 0.687, SD= 0.121). The coefficient of variation was much higher for the HMFTs for all the parameters tested and especially for the tract volume, which was the most highly variable parameter among the subjects (coefficient of variation >50%).

A factor that could contribute to the difference in the coefficient of variation is the presence of outliers. Based on Tukey's range test, only one outlier was found in the quantitative analysis of the CSTs, which was also in agreement with visual inspection. Thus, we conducted our HMFT-related quantitative analysis with all 37 subjects and then re-ran it after excluding only that one subject. The quantitative values for the HMFTs mentioned in

section 3.3, including the values depicted in Table 2, refer to the 36 subjects' measurements, given the problematic CST of the excluded subject. Contrary to our CST results that included only 1 outlier, 8 additional outliers were detected within the new total of 36 subjects in our HMFTs analysis. All the outliers were based exclusively on significant differences in the FA values. Therefore, according to our results, the FA seems to be the most sensitive parameter tested. The presence of outliers led to the higher variation noted in the HMFTs measurements.

Another finding that could provide an indication of the current capability of isolating and quantifying the hand motor area for clinical purposes regards the percentage of CST fibers belonging to the hand motor area. Based on our analysis, 12.7%, SD=5.7 of the CST fibers were HMFTs (see "(HMFT/CST) * 100 (%)" results reported in Table 2), with 11.0%, SD=9.0 for the left side and 14.5%, SD=7.3 for the right side. Once again, consistent with the high variability in determining the hand motor area using dMRI tractography, these percentages demonstrate high variance.

3.3.1 Analysis of symmetry—

Tables 1 and 2 list the SI for the left and right measurements of tract volume, length, mean FA, mean AD, and mean RD in the CST and HMFTs, respectively.

For HMFTs analysis, given that FA values and left HMFTs' volume values did not satisfy the normality assumption, a non-parametric related-samples Wilcoxon Signed Rank Test was run in SPSS, which indicated a significant difference between the FA values of the left and right hand motor region ($p<0.05$). In particular, the median FA values for the left HMFTs, median=0.69693, were significantly lower than the median FA values for the right HMFTs, median=0.71146, $Z=0.486$, $p=0.016 < 0.05$. Six of the outliers detected in our HMFTs isolation were related to asymmetrical values of FA. In particular, an absence of fibers was noted on the left side of five of the aforementioned outliers. Only one of those outliers was lacking fibers on the right side. Otherwise, no statistically significant asymmetry was found in our results.

In terms of the CST analysis, the normality assumption was satisfied, therefore we conducted a parametric paired t-test in SPSS. The test indicated no statistically significant asymmetry in the delineated CST ($p>0.05$ for all pairs tested).

3.4 Assessment of inter-subject variability of CST and HMFTs

We generated probability maps for the CSTs and HMFTs as shown in Fig. 6, following co-registration to the standard MNI152 space. The CST inter-subject variability was significantly lower in the areas adjacent to the drawn ROIs, with higher variability for the cortical areas. The inter-subject variability of the HMFTs, by contrast, seemed to be higher overall. In agreement with the CST results, cortical areas of the HMFTs were much more variable among healthy individuals.

3.5 Crossing fibers interference analysis

In an attempt to explain the apparent paucity of fibers in the hand motor area, we tested the hypothesis that crossing fibers at that anatomical level heavily affect the CST delineation, as

described in section 2.8. In agreement with our assumptions, the two sets of experiments described in section 2.8 indicated that there is an effect of the AF, SLFI, SLFII, SLFIII and CC4 (anterior midbody of the CC), as well as of the CC5 (posterior midbody of the CC), on the delineated HMFTs. Overall, based on the quantification analysis, there were no statistically significant correlations found between the volumes of the aforementioned tracts and the volumes of the HMFTs. We assume this is because of the relatively small dataset used, as well as the limitations of our correlation method, which does not allow targeted quantification and spatial correlation of overlapping fibers only. On visual inspection, however, there is an evident spatial correspondence between those tracts in the overlapping areas. In particular, the presence of denser crossing fiber tracts in the area of the HMFTs, seemed to create “openings” within the HMFTs, possibly negatively affecting the density of the delineated HMFTs. The most relevant effect seemed to be due to the SLFII, which passes exactly through the hand motor area of interest, as well as the SLFIII. The AF seemed to interfere with the lateral part of the HMFTs, whereas the SLFI appeared to affect the medial part. The CC4 and CC5 appeared to interfere heavily with the anterior and posterior parts of the HMFTs, respectively. These effects are visually illustrated in Figs. 7 and 8, where the interference of crossing fibers with the CST and, in particular with the HMFT, is explicitly depicted.

4 Discussion

In this study we performed two-tensor tractography in 36 subjects from the HCP. Using MRI identifiable, anatomically robust ROIs, namely the pyramids, cerebral peduncles and internal capsule (Makris et al. 1999; Parent 1996) we were able to delineate the CST in its entirety, as well as to isolate its hand motor representation. Furthermore, we estimated their variability and generated a database of their volume, length and biophysical parameters. We have used unscented Kalman filter based two-tensor tractography (Malcolm et al. 2010), which can robustly trace fibers through crossing fiber regions. This delineation allows for differentiation from the dense surrounding tracts in that region, namely the AF, superior longitudinal fascicles (SLFI, SLFII, SLFIII) and subdivisions of the CC. Furthermore, we assessed the anatomical variability of the CST in its entirety and the HMFTs in particular. Inter-subject variability of the HMFTs was high as mapped using probabilistic heat maps, even though such variability was not as high for the CST.

The CST is probably the most quantitatively studied fiber tract in the human brain. Traditionally, it has been estimated as composed of approximately 1 million axons, which vary from 2–11 μm in diameter. Of these axons, approximately 700,000 are myelinated and 300,000 are unmyelinated (Ford and Hackney 1997; Lassek and Rasmussen 1939; Parent 1996; Yagishita et al. 1994). Several groups have employed combinatorial approaches using both direct brain electrostimulation and DTI tractography to delineate the CST (Berman et al. 2004, 2007; Kinoshita et al. 2005; Mikuni et al. 2007). A few groups have focused instead on using only DTI tractography in order to isolate the CST (Clark et al. 2003; Itoh et al. 2006; Mandelli et al. 2014; Okada et al. 2007; Petersen et al. 2016; Yamada et al. 2005). Based on their results, the more laterally located fibers corresponding to the motor area of the hand appeared to be poorly represented or not represented at all. Recent studies (Chen et al. 2016; Farquharson et al. 2013; Mandelli et al. 2014) have raised the issue of the poor

sensitivity of currently used DTI techniques for isolating the lateral part of the CST and have suggested a potential advantage of using higher-order diffusion model tractography.

Our results are in agreement with other higher-order diffusion model tractography studies (Chen et al. 2016; Mandelli et al. 2014; Mormina et al. 2015), suggesting that DTI tractography can be a robust tool for the delineation of the CST with many potential clinical applications. Even though we previously found that the two-tensor model performed better than other popular higher-order models known to reduce false positives, given the fact that such models are more susceptible to noise (Baumgartner et al. 2012), in future work we plan to incorporate improved higher-order models into our analysis. It should be noted that, to the best of our knowledge, currently there is no tractographic approach to delineate the CST in its entirety, given the interference of other prominent crossing fiber tracts. Nevertheless, active research from several groups is focused on the problem with the aim of reaching a clinically translatable outcome (Pujol et al. 2015).

Contrary to prior studies that have attempted to isolate the hand motor area using multimodal imaging techniques or even more invasive intraoperative methodologies with electrical stimulation (Berman et al. 2004; Bucci et al. 2013; Hamidian et al. 2018; Jeong et al. 2015; Lee et al. 2016; Mandelli et al. 2014; Qazi et al. 2009; Radmanesh et al. 2015; Weiss et al. 2015), our study attempts to delineate exclusively the hand motor area of the CST and generate specific HMFTs variability maps in normal subjects, relying solely on DTI tractography. Our findings suggest that the fibers of SLF I, II and III and the AF interfere considerably with delineating the HMFTs, as shown in Figs. 4 and 7 (see e.g., https://www.ncbi.nlm.nih.gov/pmc/articles/PMC3163395/figure/F8/, https://www.ncbi.nlm.nih.gov/pmc/articles/PMC3163395/). Furthermore, crossing fibers of the CC body, CC subdivisions CC4 and CC5, seem to pose an additional obstacle to the precise evaluation of the descending HMFTs as shown in Fig. 8. The crossing fibers of these tracts appear to be the principal reason for the previously reported limitations of the tractographic algorithms to depict precisely the hand motor fibers of the CST. Supporting evidence for this view comes from studies on the clinical entity of congenital bilateral perisylvian syndrome (CBPS), a rare disease of congenital agenesis of the SLF (Bernal et al. 2010; Gropman et al. 1997; Kilinc et al. 2015; Lee et al. 2015; Saporta et al. 2011). DTI tractography performed in CBPS patients with SLF agenesis clearly isolates the hand area. Nevertheless, the trunk- and leg-related tracts could not be depicted in these studies, suggesting that other tracts might interfere with the delineation of these motor fibers (Kilinc et al. 2015). Based on our results as depicted in Fig. 6, we hypothesize that the occipitofrontal fascicle (OFF) may interfere with the trunk- and leg-related fiber tracts (Makris et al. 2007). Further studies focused on those tracts are needed to confirm our hypothesis.

4.1 Clinical significance

In this study, we were able to identify and delineate the hand motor fiber tracts in 36 healthy subjects. Although the CST appeared to be reliably sampled, given its low spatial variation it seems there were notable limitations in delineating the hand motor area fiber representation. This is highly relevant for fields such as neurorehabilitation, child and developmental

neurology, neurosurgery and neural engineering, for which more precise anatomical information may help to enable clinical advancements.

4.1.1 Clinical neurology/neurorehabilitation applications—The lack of a non-invasive neuroimaging technique that can be applied in everyday clinical practice to assess the integrity of nerve axons represents an obstacle in the evaluation and follow-up of neurological patients. Biophysical parameters such as FA value have been correlated with the integrity of nerves (Alshikho et al. 2016), and physical parameters such as number of fibers or tract volume have been correlated with nerve deficits associated with neurotrauma or disease (Feng et al. 2015). Several researchers have tried to use DTI tractography to assess the integrity of nerve fibers in neurologic conditions with motor system involvement, such as stroke (Feng et al. 2015), amyotrophic lateral sclerosis (ALS) (Graaff et al. 2011), and multiple sclerosis (MS) (Filippi et al. 2016), with results that seem promising for clinical translation. Our methodology has demonstrated very good reproducibility in order to allow the future assessment of the CST in different neurological conditions. The variability map of the CST and HMFTs that we have created based on healthy subjects could be extended further to provide a reliable and accurate reference for what is within normal range in the human population, allowing for early detection of pathologies associated with functional motor deterioration. Such future studies could compare the currently explored anatomic variability in healthy subjects to the variability in diseased subjects and supplement the results with clinical functional scales and functional imaging for the establishment of more reliable, non-invasive clinical norms. Determining and quantifying the neuroanatomical substrate of a motor deficit via our method may enable clinicians not only to monitor the progression of neurological conditions, but also to assess and quantify the effects of therapeutic and neurosurgical interventions and provide more accurate prognoses.

4.1.2 Clinical translation of novel therapeutics in neuroscience—Neurologists, neurorehabilitation physicians and neural engineers are currently moving toward clinical translation of neural repair and neuroprotection strategies for CNS trauma and disease, such as traumatic brain injury (TBI) (Aertker et al. 2016), stroke (Manley et al. 2015), ALS (Petrou et al. 2016) and SCI (Lu et al. 2016). Nevertheless, in order to quantify and assess the effects of such novel therapeutics in neurological patients, non-invasive, reliable in vivo techniques are key for progressing to a safe clinical translation. Our method could easily be implemented in clinical studies in order to assess and quantify the response of neural tissue to new therapeutic interventions that are progressing to clinical trials.

5 Limitations and future studies

5.1 Study-specific limitations

Our dataset is a HCP high-resolution dataset, meaning that our results may not be reproduced in lower resolution clinical datasets. Thus, further validation is needed with datasets of differing resolutions. It should be noted that a larger dataset testing different acquisition parameters or use of the future HCP disease datasets (https://www.humanconnectome.org/disease-studies) might affect the diffusion MRI tractography

analysis parameters and the associated reliability reported, which would be an interesting topic for future investigation. Nevertheless, the focus of the current study is limited to healthy human subjects in order to explore the anatomy of the CST and HMFT in the individual subject and determine the variability within healthy populations, using a high-resolution dataset for increased accuracy.

In addition, we chose to use a delineation methodology based on the drawing of manual ROIs in order to obtain the most accurate and clinically applicable results. For the purpose of the present study, this significantly increased accuracy and precision is important for establishing accurate variability maps in the healthy population. However, in future studies with large data cohorts (such as HCP with 1200 subjects) we may need to consider a machine-learning approach in order to facilitate the implementation of such methodology to make it feasible to perform such studies on a large scale. Although biophysical properties of diffusion imaging could be influenced by several factors such as age or sex, given that in this study we focused on topographical anatomical variability, we do not think our variability results would be affected by these factors. The choice of two-tensor UKF tractography might be highly useful for addressing some of the crossing-fiber tractography-related obstacles in order to allow better delineation of fiber tracts. However, the tractography is still limited to tracing only two-fiber crossings and cannot trace fibers that pass through three-fiber crossings, which may contribute to increased variability of the tracts traced. Our future work will involve using more sophisticated algorithms that can address these shortcomings.

Finally, although we think the functional characterization of the hand motor area is a highly relevant issue, this is outside of the scope of the present study, which is focused on elucidating the structural variability of the HMFT. If we were to correlate functional data derived from a hand motor task as in the HCP datasets, such a task would not be purely motor but also somatosensory. Thus, in correlating DTI biophysical parameters with functional motor tasks we would not expect to add any new understanding with respect to the anatomical and topographic variability of the HMFT per se, which is our principal focus here. Furthermore, the HCP datasets used in this study comprise healthy subjects, and we have not compared healthy versus diseased populations.

5.2 Technical considerations

Although we have selected datasets from healthy human subjects from the Connectome scanners considered to have the highest signal-to-noise ratio and resolution standards currently in the world, a future change in the resolution of acquisition or higher field strengths may affect the results (Alexander et al. 2001). Optimal parameters for visualizing tracts and nerve fibers remain to be developed.

There are well-known and well described limitations to the tractography methods used in the present study. As mentioned above, tract volume and FA values in DTI tractography can vary within and across subjects (Catani 2007; Heiervang et al. 2006), which necessitates that large numbers of subjects be studied to draw more accurate and clinically applicable conclusions. In addition, false positive or false negative results have been reported in tractography (Farquharson et al. 2013; Jones et al. 2013; O'Donnell and Pasternak 2015; O'Donnell and Westin 2011). Thus, we tried to ensure that our analysis was based on valid

and reliable anatomic landmarks using manually drawn ROIs and a robust quality control analysis with optimization of the tractography algorithm parameters for the particular high-resolution dataset. Based on the significant problem of crossing fibers as discussed above, two-tensor UKF tractography was chosen in order to minimize the effect of crossing fibers in our dataset as much as possible. Finally, a limitation of tractography especially relevant to neurosurgeons is that although it gives a good estimate of a fiber tract representation spatially, it provides neither the actual representation of the volume of the tract nor the number of fibers (Kinoshita et al. 2005; Nimsky et al. 2016). Thus, careful implementation and interpretation of tractography-based techniques is advised for neurosurgical applications.

6 Conclusions

We have demonstrated that two-tensor UKF tractography could be a robust tool for motor pathway isolation, in particular the CST and HFMT, significantly improving the tracking of tracts and overcoming certain intrinsic limitations of DTI tractography (i.e. crossing fibers or, as in other reports, peritumoral edema) as a higher-order model tractography algorithm. CST variability was delineated in healthy subjects using state-of-the-art HCP data in order to serve as a reference for future anatomical studies and for establishing clinical correlations by neurorehabilitation physicians, neurologists, and neurosurgeons. The HMFTs were also isolated for the first time using solely DTI tractography. A healthy-subjects' inter-subject variability heat map was described to allow future validation and improvement of the technique and imaging modalities and algorithms, given the great importance of this motor area for clinicians. Even though variance was much higher for the HMFTs than the CST, partially due to the presence of outliers, our methodology seems appropriate for the isolation of HMFTs in small group studies. Nevertheless, there remains significant need for improvement of the tools in order to ensure reliable single-subject analysis of the CST and HMFT in clinical settings. Further validation of the current results with a greater number of subjects is needed to establish an accurate variability map that can be used reliably for the clinical screening of fiber tract pathologies and to track neuroregenerative processes.

Acknowledgements

We would like to thank the anonymous reviewers for providing useful comments on the manuscript. We would also like to thank Prof. Myron Spector for fruitful discussions and for his support.

Funding

K.D. was partially supported by the Foundation for Education and European Culture (IPEP). M.T. was supported by the American Association of University Women (AAUW) and the Onassis Foundation. E.Y. was supported by Colby College Research Fund 01 2836. NIH P41 EB015902. P.S. was supported by a NARSAD Young Investigator Award, grant number 22591 from the Brain and Behavior Research Foundation. N.M. was supported by RO1AG042512 (National Institute of Aging & National Institute of Mental Health), RO1MH112748 (National Institute of Mental Health), RO1MH111917 (National Institute of Mental Health), R21AT008865 (National Center for Complementary and Integrative Health), R21DA042271 (National Institute of Drug Abuse), and K24MH116366 (National Institute of Mental Health).

Abbreviations:

CST

corticospinal tract

HMFT(s)
hand-related motor fiber tract(s)

PT
pyramidal tract

BA
Brodmann area

dMRI
diffusion magnetic resonance imaging

DTI
diffusion tensor imaging

HARDI
high angular resolution diffusion imaging

IC
internal capsule

SCI
spinal cord injury

TBI
traumatic brain injury

MS
multiple sclerosis

ALS
amyotrophic lateral sclerosis

AF
arcuate fascicle

SLF
superior longitudinal fascicle

CC
corpus callosum

HCP
Human Connectome Project

UKF
deterministic tractography - unscented Kalman filter deterministic tractography

FA
fractional anisotropy

AD
axial diffusivity

RD
radial diffusivity

SD
standard deviation

WU-Minn HCP consortium
Washington University-University of Minnesota and Oxford University Human Connectome Project consortium

ROIs
regions of interest

WMQL
White Matter Query Language

AC
anterior commissure

SI
Symmetry index

WashU
Washington University

MNI
Montreal Neurological Institute

CBPS
congenital bilateral perisylvian syndrome

OFF
occipitofrontal fascicle

References

Aertker BM, Bedi S, & Cox CS Jr (2016). Strategies for CNS repair following TBI. Experimental Neurology, 275(3), 411–426. doi:10.1016/j.expneurol.2015.01.008 [PubMed: 25637707]

Alexander AL, Hasan KM, Lazar M, Tsuruda JS, & Parker DL (2001). Analysis of partial volume effects in diffusion-tensor MRI. Magnetic Resonance in Medicine, 45(5), 770–780. [PubMed: 11323803]

Alshikho MJ, Zürcher NR, Loggia ML, Cernasov P, Chonde DB, Izquierdo Garcia D, et al. (2016). Glial activation colocalizes with structural abnormalities in amyotrophic lateral sclerosis. Neurology, 87(24), 2554–2561. doi:10.1212/WNL.0000000000003427 [PubMed: 27837005]

Barnard JW, & Woolsey CN (1956). A study of localization in the corticospinal tracts of monkey and rat. Journal of Comparative Neurology, 105(1), 25–50. [PubMed: 13367242]

Basser PJ (2004). Scaling laws for myelinated axons derived from an electrotonic core-conductor model. Journal of Integrative Neuroscience, 3(2), 227–244. [PubMed: 15285056]

Basser PJ, Mattiello J, & LeBihan D (1994). MR diffusion tensor spectroscopy and imaging. Biophysical Journal, 66(1), 259–267. [PubMed: 8130344]

Baumgartner CF, Michailovich O, Levitt J, Pasternak O, Bouix S, Westin CF, & Rathi Y (2012). A unified tractography framework for comparing diffusion models on clinical scans. Presented at the CDMRI Workshop-MICCAI '12, Nice, France.

Berman JI, Berger MS, Chung S, Nagarajan SS, & Henry RG (2007). Accuracy of diffusion tensor magnetic resonance imaging tractography assessed using intraoperative subcortical stimulation mapping and magnetic source imaging. Journal of Neurosurgery, 107(3), 488–494. doi:10.3171/JNS-07/09/0488 [PubMed: 17886545]

Berman JI, Berger MS, Mukherjee P, & Henry RG (2004). Diffusion-tensor imaging-guided tracking of fibers of the pyramidal tract combined with intraoperative cortical stimulation mapping in patients with gliomas. Journal of Neurosurgery, 101(1), 66–72. doi:10.3171/jns.2004.101.1.0066 [PubMed: 15255253]

Berman JI, Lanza MR, Blaskey L, Edgar JC, & Roberts TPL (2013). High angular resolution diffusion imaging (HARDI) probabilistic tractography of the auditory radiation. American Journal of Neuroradiology, 34(8), 1573–1578. doi:10.3174/ajnr.A3471 [PubMed: 23493892]

Bernal B, Rey G, Dunoyer C, Shanbhag H, & Altman N (2010). Agenesis of the arcuate fasciculi in congenital bilateral perisylvian syndrome: A diffusion tensor imaging and tractography study. Archives of Neurology, 67(4), 501–505. doi:10.1001/archneurol.2010.59 [PubMed: 20385920]

Bertrand G, Blundell J, & Musella R (1965). Electrical exploration of the internal capsule and neighbouring structures during stereotaxic procedures. Journal of Neurosurgery, 22(4), 333–343. [PubMed: 14318109]

Betz W (1874). Anatomischer Nachweis zweier Gehirncentra. Zentralblatt für die medizinischen Wissenschaften, 12, 578–580; 595–599.

Bouchard C (1866). Secondary degenerations of the spinal cord. Translated into English by E.R. Hun (Utica, NY 1869) Cited by A. M. Lassek, The pyramidal tract (Springfield, IL: Thomas 1954).

Bucci M, Mandelli ML, Berman JI, Amirbekian B, Nguyen C, Berger MS, & Henry RG (2013). Quantifying diffusion MRI tractography of the corticospinal tract in brain tumors with deterministic and probabilistic methods. NeuroImage: Clinical, 3, 361–368. doi:10.1016/j.nicl.2013.08.008 [PubMed: 24273719]

Caiazzo G, Fratello M, Di Nardo F, Trojsi F, Tedeschi G, & Esposito F (2018). Structural connectome with high angular resolution diffusion imaging MRI: Assessing the impact of diffusion weighting and sampling on graph-theoretic measures. Neuroradiology, 60(5), 497–504. doi:10.1007/s00234-018-2003-7 [PubMed: 29520641]

Campbell AW (1905). Histological studies on the localization of cerebral function. Cambridge, England: Cambridge University Press.

Carlson HL, Laliberté C, Brooks BL, Hodge J, Kirton A, Bello-Espinosa L, et al. (2014). Reliability and variability of diffusion tensor imaging (DTI) tractography in pediatric epilepsy. Epilepsy & Behavior, 37, 116–122. doi:10.1016/j.yebeh.2014.06.020 [PubMed: 25014749]

Catani M (2007). From hodology to function. Brain, 130(3), 602–605. doi:10.1093/brain/awm008 [PubMed: 17322561]

Chen Z, Tie Y, Olubiyi O, Zhang F, Mehrtash A, Rigolo L, et al. (2016). Corticospinal tract modeling for neurosurgical planning by tracking through regions of peritumoral edema and crossing fibers using two-tensor unscented Kalman filter tractography. International Journal of Computer Assisted Radiology and Surgery, 11(8), 1475–1486. doi:10.1007/s11548-015-1344-5 [PubMed: 26762104]

Chronister RB, & Hardy SGP (1997). The limbic system In Haines DE (Ed.), Fundamental neuroscience (pp. 443–454). London: Churchill Livingstone.

Clark CA, Barrick TR, Murphy MM, & Bell BA (2003). White matter fiber tracking in patients with space-occupying lesions of the brain: a new technique for neurosurgical planning? NeuroImage, 20(3), 1601–1608. doi:10.1016/j.neuroimage.2003.07.022 [PubMed: 14642471]

Clarke E, & O'Malley CD (1996). The human brain and spinal cord: A historical study illustrated by writings from antiquity to the twentieth century (2nd ed.). San Francisco: Norman Publishing.

Cronbach LJ (1951). Coefficient alpha and the internal structure of tests. Psychometrika, 16(3), 297–334. doi:10.1007/BF02310555

Cruveilhier J (1853). Sur la paralysie musculaire progressive atrophique. Archives Générales de Médecine, 1, 561–603.

Davidoff RA (1990). The pyramidal tract. Neurology, 40(2), 332–332. [PubMed: 2405296]

Dejerine JJ, & Dejerine-Klumpke A (1895). Anatomie des centres nerveux (Vol. 1). Paris Rueff et Cie.

Dini L, Vedolin L, Bertholdo D, Grando R, Mazzola A, Dini S, et al. (2013). Reproducibility of quantitative fiber tracking measurements in diffusion tensor imaging of frontal lobe tracts: A protocol based on the fiber dissection technique. Surgical Neurology International, 4(1), 51. doi:10.4103/2152-7806.110508 [PubMed: 23646261]

Ellis CM, Suckling J, Amaro E Jr, Bullmore ET, Simmons A, Williams SCR, & Leigh PN (2001). Volumetric analysis reveals corticospinal tract degeneration and extramotor involvement in ALS. Neurology, 57(9), 1571–1578. [PubMed: 11706094]

Farquharson S, Tournier JD, Calamante F, Fabinyi G, Schneider-Kolsky M, Jackson GD, & Connelly A (2013). White matter fiber tractography: Why we need to move beyond DTI. Journal of Neurosurgery, 118(6), 1367–1377. doi:10.3171/2013.2.JNS121294 [PubMed: 23540269]

Fedorov A, Beichel R, Kalpathy-Cramer J, Finet J, Fillion-Robin JC, Pujol S, et al. (2012). 3D Slicer as an image computing platform for the Quantitative Imaging Network. Magnetic Resonance Imaging, 30(9), 1323–1341. doi:10.1016/j.mri.2012.05.001 [PubMed: 22770690]

Feng W, Wang J, Chhatbar PY, Doughty C, Landsittel D, Lioutas VA, et al. (2015). Corticospinal tract lesion load: An imaging biomarker for stroke motor outcomes. Annals of Neurology, 78(6), 860–870. doi:10.1002/ana.24510 [PubMed: 26289123]

Filippi M, Pagani E, Preziosa P, & Rocca MA (2016). The role of DTI in multiple sclerosis and other demyelinating conditions In Hecke WV, Emsell L, & Sunaert S (Eds.), Diffusion tensor imaging (pp. 331–341). New York: Springer. doi:10.1007/978-1-4939-3118-7_16

Finger S (1994). Origins of neuroscience: A history of explorations into brain function. New York: Oxford University Press.

Flechsig PE (1877). Pyramidal tract in brain and cord. Archiv für der Heilkunde, 18, 101–141..

Flechsig PE (1904). Einige Bemerkungen über die Untersuchungsmethoden der Grosshirnrinde, insbesondere des Menschen. Berichie über die Verhandlungen der Sächsischen Akademie der Wissenschaften zu Leipzig, Mathematik-Physik Klasse, 56, 50–104; 177–248.

Ford JC, & Hackney DB (1997). Numerical model for calculation of apparent diffusion coefficients (ADC) in permeable cylinders: Comparison with measured ADC in spinal cord white matter. Magnetic Resonance in Medicine, 37(3), 387–394. doi:10.1002/mrm.1910370315 [PubMed: 9055229]

Galaburda AM, Corsiglia J, Rosen GD, & Sherman GF (1987). Planum temporale asymmetry, reappraisal since Geschwind and Levitsky. Neuropsychologia, 25(6), 853–868. doi:10.1016/0028-3932(87)90091-1

Gall FJ, & Spurzheim JC (1810). Anatomie et physiologie du système nerveux en général, et du cerveau en particuler. Paris: Schoell et al.

Glasser MF, Sotiropoulos SN, Wilson JA, Coalson TS, Fischl B, Andersson JL, et al. (2013). The minimal preprocessing pipelines for the Human Connectome Project. NeuroImage, 80, 105–124. doi:10.1016/j.neuroimage.2013.04.127 [PubMed: 23668970]

Graaff MM van der, Sage CA, Caan MWA, Akkerman EM, Lavini C, Majoie CB, et al. (2011). Upper and extra-motoneuron involvement in early motoneuron disease: a diffusion tensor imaging study. Brain, 134(4), 1211–1228. doi:10.1093/brain/awr016 [PubMed: 21362631]

Gropman AL, Barkovich AJ, Vezina LG, Conry JA, Dubovsky EC, & Packer RJ (1997). Pediatric congenital bilateral perisylvian syndrome: clinical and MRI features in 12 patients. Neuropediatrics, 28(4), 198–203. doi:10.1055/s-2007-973700 [PubMed: 9309709]

Hamidian S, Vachha B, Jenabi M, Karimi S, Young RJ, Holodny AI, & Peck KK (2018). Resting state fMRI and probabilistic DTI demonstrate that the greatest functional and structural connectivity in

the hand motor homunculus occurs in the area of the thumb. Brain Connectivity, 10.1089/brain.2018.0589

Heiervang E, Behrens TEJ, Mackay CE, Robson MD, & Johansen-Berg H (2006). Between session reproducibility and between subject variability of diffusion MR and tractography measures. NeuroImage, 33(3), 867–877. doi:10.1016/j.neuroimage.2006.07.037 [PubMed: 17000119]

Hille B (2001). Ion channels of excitable membranes (3rd ed.). Sunderland, MA: Sinauer Associates Inc.

Hirayama K, Tsubaki T, Toyokura Y, & Okinaka S (1962). The representation of the pyramidal tract in the internal capsule and basis pedunculi: A study based on three cases of amyotrophic lateral sclerosis. Neurology, 12, 337. [PubMed: 13907643]

Holmes G, & May WP (1909). On the exact origin of the pyramidal tracts in man and other mammals. Brain, 32(1), 1–43.

Holodny AI, Gor DM, Watts R, Gutin PH, & Ulug AM (2005). Diffusion-tensor MR tractography of somatotopic organization of corticospinal tracts in the internal capsule: Initial anatomic results in contradistinction to prior reports. Radiology, 234(3), 649–653. [PubMed: 15665224]

Huang H, Zhang J, Jiang H, Wakana S, Poetscher L, Miller MI, et al. (2005). DTI tractography based parcellation of white matter: Application to the mid-sagittal morphology of corpus callosum. NeuroImage, 26(1), 195–205. doi:10.1016/j.neuroimage.2005.01.019 [PubMed: 15862219]

Irfanoglu MO, Modi P, Nayak A, Hutchinson EB, Sarlls J, & Pierpaoli C (2015). DR-BUDDI (Diffeomorphic Registration for Blip-Up blip-Down Diffusion Imaging) method for correcting echo planar imaging distortions. NeuroImage, 106, 284–299. doi:10.1016/j.neuroimage.2014.11.042 [PubMed: 25433212]

Itoh D, Aoki S, Maruyama K, Masutani Y, Mori H, Masumoto T, et al. (2006). Corticospinal tracts by diffusion tensor tractography in patients with arteriovenous malformations. Journal of Computer Assisted Tomography, 30(4), 618–623. [PubMed: 16845293]

Jeong JW, Lee J, Kamson DO, Chugani HT, & Juhász C (2015). Detection of hand and leg motor tract injury using novel diffusion tensor MRI tractography in children with central motor dysfunction. Magnetic Resonance Imaging, 33(7), 895–902. doi:10.1016/j.mri.2015.05.003 [PubMed: 25959649]

Jones DK, Knösche TR, & Turner R (2013). White matter integrity, fiber count, and other fallacies: The do's and don'ts of diffusion MRI. NeuroImage, 73, 239–254. doi:10.1016/j.neuroimage.2012.06.081 [PubMed: 22846632]

Kilinc O, Ekinci G, Demirkol E, & Agan K (2015). Bilateral agenesis of arcuate fasciculus demonstrated by fiber tractography in congenital bilateral perisylvian syndrome. Brain & Development, 37(3), 352–355. doi:10.1016/j.braindev.2014.05.003 [PubMed: 24852949]

Kinoshita M, Yamada K, Hashimoto N, Kato A, Izumoto S, Baba T, et al. (2005). Fiber-tracking does not accurately estimate size of fiber bundle in pathological condition: initial neurosurgical experience using neuronavigation and subcortical white matter stimulation. NeuroImage, 25(2), 424–429. doi:10.1016/j.neuroimage.2004.07.076 [PubMed: 15784421]

Kuo H, Ferre CL, Carmel JB, Gowatsky JL, Stanford AD, Rowny SB, et al. (2017). Using diffusion tensor imaging to identify corticospinal tract projection patterns in children with unilateral spastic cerebral palsy. Developmental Medicine and Child Neurology, 59(1), 65–71. doi:10.1111/dmcn.13192 [PubMed: 27465858]

Kuypers H (1958). Some projections from the peri-central cortex to the pons and lower brain stem in monkey and chimpanzee. Journal of Comparative Neurology, 110(2), 221–255. [PubMed: 13654557]

Kuypers HG (1964). The descending pathways to the spinal cord, their anatomy and function. Progress in Brain Research, 11, 178–202. [PubMed: 14300477]

Lassek AM, & Rasmussen GL (1939). The human pyramidal tract: A fiber and numerical analysis. Archives of Neurology & Psychiatry, 42(5), 872–876.

Le Bihan D, Breton E, Lallemand D, Grenier P, Cabanis E, & Laval-Jeantet M (1986). MR imaging of intravoxel incoherent motions: Application to diffusion and perfusion in neurologic disorders. Radiology, 161(2), 401–407. [PubMed: 3763909]

Le Gros Clark WE (1959). The antecedents of man: An introduction to the evolution of the primates. Edinburgh: Edinburgh University Press.

Lee DH, Lee DW, & Han BS (2016). Symmetrical location characteristics of corticospinal tract associated with hand movement in the human brain. Medicine, 95(15), e3317. doi:10.1097/MD.0000000000003317 [PubMed: 27082576]

Lee DH, Park JW, Park SH, & Hong C (2015). Have you ever seen the impact of crossing fiber in DTI?: Demonstration of the corticospinal tract pathway. PLoS ONE, 10(7). doi:10.1371/journal.pone.0112045

Levin PM, & Beadford FK (1938). The exact origin of the cortico-spinal tract in the monkey. Journal of Comparative Neurology, 68(4), 411–422.

Lori NF, Akbudak E, Shimony JS, Cull TS, Snyder AZ, Guillory RK, & Conturo TE (2002). Diffusion tensor fiber tracking of human brain connectivity: Acquisition methods, reliability analysis and biological results. NMR in Biomedicine, 15(7–8), 494–515. [PubMed: 12489098]

Lu P, Ahmad R, & Tuszynski MH (2016). Neural stem cells for spinal cord injury In Tuszynski MH (Ed.), Translational neuroscience (pp. 297–315). New York: Springer. doi:10.1007/978-1-4899-7654-3_16

Mai JK, & Paxinos G (2011). The human nervous system (3rd ed.). New York: Academic Press.

Makris N, Worth AJ, Papadimitriou GM, Stakes JW, Caviness VS, Kennedy DN, et al. (1997). Morphometry of in vivo human white matter association pathways with diffusion-weighted magnetic resonance imaging. Annals of Neurology, 42(6), 951–962. [PubMed: 9403488]

Makris N, Kennedy DN, McInerney S, Sorensen AG, Wang R, Caviness VS, & Pandya DN (2005). Segmentation of subcomponents within the superior longitudinal fascicle in humans: A quantitative, in vivo, DT-MRI study. Cerebral Cortex, 15(6), 854–869. doi:10.1093/cercor/bhh186 [PubMed: 15590909]

Makris N, Meyer JW, Bates JF, Yeterian EH, Kennedy DN, & Caviness VS Jr. (1999). MRI-based topographic parcellation of human cerebral white matter and nuclei: II. Rationale and applications with systematics of cerebral connectivity. NeuroImage, 9(1), 18–45. doi:10.1006/nimg.1998.0384 [PubMed: 9918726]

Makris N, Papadimitriou GM, Sorg S, Kennedy DN, Caviness VS, & Pandya DN (2007). The occipitofrontal fascicle in humans: a quantitative, in vivo, DT-MRI study. NeuroImage, 37(4), 1100–1111. doi:10.1016/j.neuroimage.2007.05.042 [PubMed: 17681797]

Malcolm JG, Shenton ME, & Rathi Y (2010). Filtered multitensor tractography. IEEE Transactions on Medical Imaging, 29(9), 1664–1675. doi:10.1109/TMI.2010.2048121 [PubMed: 20805043]

Mandelli ML, Berger MS, Bucci M, Berman JI, Amirbekian B, & Henry RG (2014). Quantifying accuracy and precision of diffusion MR tractography of the corticospinal tract in brain tumors. Journal of Neurosurgery, 121(2), 349–358. doi:10.3171/2014.4.JNS131160 [PubMed: 24905560]

Manley NC, Azevedo-Pereira RL, Bliss TM, & Steinberg GK (2015). Neural stem cells in stroke: Intracerebral approaches In Hess DC (Ed.), Cell therapy for brain injury (pp. 91–109). New York: Springer. doi:10.1007/978-3-319-15063-5_7

Mikuni N, Okada T, Enatsu R, Miki Y, Hanakawa T, Urayama S, et al. (2007). Clinical impact of integrated functional neuronavigation and subcortical electrical stimulation to preserve motor function during resection of brain tumors. Journal of Neurosurgery, 106(4), 593–598. doi:10.3171/jns.2007.106.4.593 [PubMed: 17432708]

Mori S, Crain BJ, Chacko VP, & Van Zijl P (1999). Three-dimensional tracking of axonal projections in the brain by magnetic resonance imaging. Annals of Neurology, 45(2), 265–269. [PubMed: 9989633]

Mormina E, Longo M, Arrigo A, Alafaci C, Tomasello F, Calamuneri A, et al. (2015). MRI tractography of corticospinal tract and arcuate fasciculus in high-grade gliomas performed by constrained spherical deconvolution: Qualitative and quantitative analysis. American Journal of Neuroradiology, 36(10), 1853–1858. doi:10.3174/ajnr.A4368 [PubMed: 26113071]

Nimsky C, Bauer M, & Carl B (2016). Merits and limits of tractography techniques for the uninitiated In Schramm J (Ed.), Advances and technical standards in neurosurgery (pp. 37–60). New York: Springer. doi:10.1007/978-3-319-21359-0_2

Norton I, Essayed WI, Zhang F, Pujol S, Yarmarkovich A, Golby A, et al. (2017). SlicerDMRI: Open Source Diffusion MRI Software for Brain Cancer Research. Cancer Research, 77(21), e101–e103. doi:10.1158/0008-5472.CAN-17-0332 [PubMed: 29092950]

Nyberg-Hansen R, & Rinvik E (1963). Some comments on the pyramidal tract, with special reference to its individual variations in man. Acta Neurologica Scandinavica, 39(1), 1–30.

O'Donnell LJ, & Pasternak O (2015). Does diffusion MRI tell us anything about the white matter? An overview of methods and pitfalls. Schizophrenia Research, 161(1), 133–141. doi:10.1016/j.schres.2014.09.007 [PubMed: 25278106]

O'Donnell LJ, & Westin CF (2011). An introduction to diffusion tensor image analysis. Neurosurgery Clinics of North America, 22(2), 185–196, viii. doi:10.1016/j.nec.2010.12.004 [PubMed: 21435570]

Okada T, Miki Y, Kikuta K, Mikuni N, Urayama S, Fushimi Y, et al. (2007). Diffusion tensor fiber tractography for arteriovenous malformations: Quantitative analyses to evaluate the corticospinal tract and optic radiation. American Journal of Neuroradiology, 28(6), 1107–1113. doi:10.3174/ajnr.A0493 [PubMed: 17569969]

Parent A (1996). Carpenter's human neuroanatomy (9th ed.). Baltimore: Williams & Wilkins.

Peele TL (1942). Cytoarchitecture of individual parietal areas in the monkey (Macaca mulatta) and the distribution of the efferent fibers. Journal of Comparative Neurology, 77(3), 693–737.

Pellegrino RG, Spencer PS, & Ritchie JM (1984). Sodium channels in the axolemma of unmyelinated axons: a new estimate. Brain Research, 305(2), 357–360. doi:10.1016/0006-8993(84)90442-6 [PubMed: 6331604]

Petersen MV, Lund TE, Sunde N, Frandsen J, Rosendal F, Juul N, & Østergaard K (2016). Probabilistic versus deterministic tractography for delineation of the cortico-subthalamic hyperdirect pathway in patients with Parkinson disease selected for deep brain stimulation. Journal of Neurosurgery, 126(5), 1657–1668. doi:10.3171/2016.4.JNS1624 [PubMed: 27392264]

Petrou P, Gothelf Y, Argov Z, Gotkine M, Levy YS, Kassis I, et al. (2016). Safety and clinical effects of mesenchymal stem cells secreting neurotrophic factor transplantation in patients with amyotrophic lateral sclerosis: Results of phase 1/2 and 2a clinical trials. JAMA Neurology, 73(3), 337–344. doi:10.1001/jamaneurol.2015.4321 [PubMed: 26751635]

Pierpaoli C, Barnett A, Pajevic S, Chen R, Penix L, Virta A, & Basser P (2001). Water diffusion changes in Wallerian degeneration and their dependence on white matter architecture. Neuroimage, 13(6), 1174–1185. [PubMed: 11352623]

Pitres JA (1884). Recherches anatomo-cliniques sur les scléroses bilatérales de la moelle épinière consécutives à des lésions unilatérales du cerveau. Paris: G. Masson.

Pujol S, Wells W, Pierpaoli C, Brun C, Gee J, Cheng G, et al. (2015). The DTI challenge: Toward standardized evaluation of diffusion tensor imaging tractography for neurosurgery. Journal of Neuroimaging, 25(6), 875–882. doi:10.1111/jon.12283 [PubMed: 26259925]

Qazi AA, Radmanesh A, O'Donnell L, Kindlmann G, Peled S, Whalen S, et al. (2009). Resolving crossings in the corticospinal tract by two-tensor streamline tractography: Method and clinical assessment using fMRI. NeuroImage, 47(Suppl. 2), T98–T106. doi:10.1016/j.neuroimage.2008.06.034 [PubMed: 18657622]

Radmanesh A, Zamani AA, Whalen S, Tie Y, Suarez RO, & Golby AJ (2015). Comparison of seeding methods for visualization of the corticospinal tracts using single tensor tractography. Clinical Neurology and Neurosurgery, 129, 44–49. doi:10.1016/j.clineuro.2014.11.021 [PubMed: 25532134]

Ropper AH, Samuels MA, & Klein J (2014). Adams and Victor's principles of neurology (10th ed.). New York: McGraw-Hill Education.

Russell JR, & DeMyer W (1961). The quantitative cortical origin of pyramidal axons of Macaca rhesus with some remarks on the slow rate of axolysis. Neurology, 11(2), 96–96.

Saporta ASD, Kumar A, Govindan RM, Sundaram SK, & Chugani HT (2011). Arcuate fasciculus and speech in congenital bilateral perisylvian syndrome. Pediatric Neurology, 44(4), 270–274. doi:10.1016/j.pediatrneurol.2010.11.006 [PubMed: 21397168]

Schäfer EA (1883). Report on the lesions, primary and secondary, in the brain and spinal cord of the macacque monkey, exhibited by professors Ferrier and Yeo. Journal of Physiology 4(4–5), 316–326.

Schäfer EA (1910). Experiments on the paths taken by volitional impulses passing from the cerebral cortex to the cord: The pyramids and the ventro-laterla descending tracts. Quarterly Journal of Experimental Physiology, 3(4), 355–373.

Schmahmann JD, & Pandya DN (2006). Fiber pathways of the brain. New York: Oxford Univeristy Press.

Sherbondy AJ, Dougherty RF, Napel S, & Wandell BA (2008). Identifying the human optic radiation using diffusion imaging and fiber tractography. Journal of Vision, 8(10), 12.1–1211. doi:10.1167/8.10.12

Skirven TM, Osterman AL, Fedorczyk J, & Amadio PC (2011). Rehabilitation of the hand and upper extremity (6th ed.). Philadelphia: Elsevier Mosley.

Snow NJ, Peters S, Borich MR, Shirzad N, Auriat AM, Hayward KS, & Boyd LA (2016). A reliability assessment of constrained spherical deconvolution-based diffusion-weighted magnetic resonance imaging in individuals with chronic stroke. Journal of Neuroscience Methods, 257, 109–120. doi:10.1016/j.jneumeth.2015.09.025 [PubMed: 26434704]

Song SK, Sun SW, Ju WK, Lin SJ, Cross AH, & Neufeld AH (2003). Diffusion tensor imaging detects and differentiates axon and myelin degeneration in mouse optic nerve after retinal ischemia. NeuroImage, 20(3), 1714–1722. [PubMed: 14642481]

Song SK, Sun SW, Ramsbottom MJ, Chang C, Russell J, & Cross AH (2002). Dysmyelination revealed through MRI as increased radial (but unchanged axial) diffusion of water. NeuroImage, 17(3), 1429–1436. [PubMed: 12414282]

Stieltjes B, Kaufmann WE, van Zijl PC, Fredericksen K, Pearlson GD, Solaiyappan M, & Mori S (2001). Diffusion tensor imaging and axonal tracking in the human brainstem. NeuroImage, 14(3), 723–735. doi:10.1006/nimg.2001.0861 [PubMed: 11506544]

Tuch DS, Reese TG, Wiegell MR, Makris N, Belliveau JW, & Wedeen VJ (2002). High angular resolution diffusion imaging reveals intravoxel white matter fiber heterogeneity. Magnetic Resonance in Medicine, 48(4), 577–582. [PubMed: 12353272]

Tukey JW (1977). Exploratory Data Analysis. Reading, MA: Pearson.

Türck L (1851). Über den Zustand der Sensibilität nach teilweiser Trennung des Rückenmarks. Zeitschrift für die Gesellschaft der Aerzte zu Wien, 189.

Uğurbil K, Xu J, Auerbach EJ, Moeller S, Vu A, Duarte-Carvajalino JM, et al. (2013). Pushing spatial and temporal resolution for functional and diffusion MRI in the Human Connectome Project. NeuroImage, 80, 80–104. doi:10.1016/j.neuroimage.2013.05.012 [PubMed: 23702417]

Wassermann D, Makris N, Rathi Y, Shenton M, Kikinis R, Kubicki M, & Westin CF (2013). On Describing human white matter anatomy: The White Matter Query Language. Medical Image Computing and Computer Assisted Intervention, 16(0 1), 647–654. [PubMed: 24505722]

Wassermann D, Makris N, Rathi Y, Shenton M, Kikinis R, Kubicki M, & Westin CF (2016). The white matter query language: A novel approach for describing human white matter anatomy. Brain Structure and Function, 221(9), 4705–4721. doi:10.1007/s00429-015-1179-4 [PubMed: 26754839]

Weiss C, Tursunova I, Neuschmelting V, Lockau H, Nettekoven C, Oros-Peusquens AM, et al. (2015). Improved nTMS- and DTI-derived CST tractography through anatomical ROI seeding on anterior pontine level compared to internal capsule. NeuroImage: Clinical, 7, 424–437. doi:10.1016/j.nicl.2015.01.006 [PubMed: 25685709]

Willis T (1664). Cerebri anatome: Cui accessit nervorum descriptio et usus London: Martyn J and Allestry J. Tercentenary ed., 1664–1964, Thomas Willis: The anatomy of the brain and nerves. Montreal: McGill University Press, 1965.

Yagishita A, Nakano I, Oda M, & Hirano A (1994). Location of the corticospinal tract in the internal capsule at MR imaging. Radiology, 191(2), 455–460. [PubMed: 8153321]

Yamada K, Kizu O, Ito H, Kubota T, Akada W, Goto M, et al. (2005). Tractography for arteriovenous malformations near the sensorimotor cortices. American Journal of Neuroradiology, 26(3), 598–602. [PubMed: 15760872]

Yousry TA, Schmid UD, Alkadhi H, Schmidt D, Peraud A, Buettner A, & Winkler P (1997). Localization of the motor hand area to a knob on the precentral gyrus: A new landmark. Brain, 120(1), 141–157. doi:10.1093/brain/120.1.141 [PubMed: 9055804]

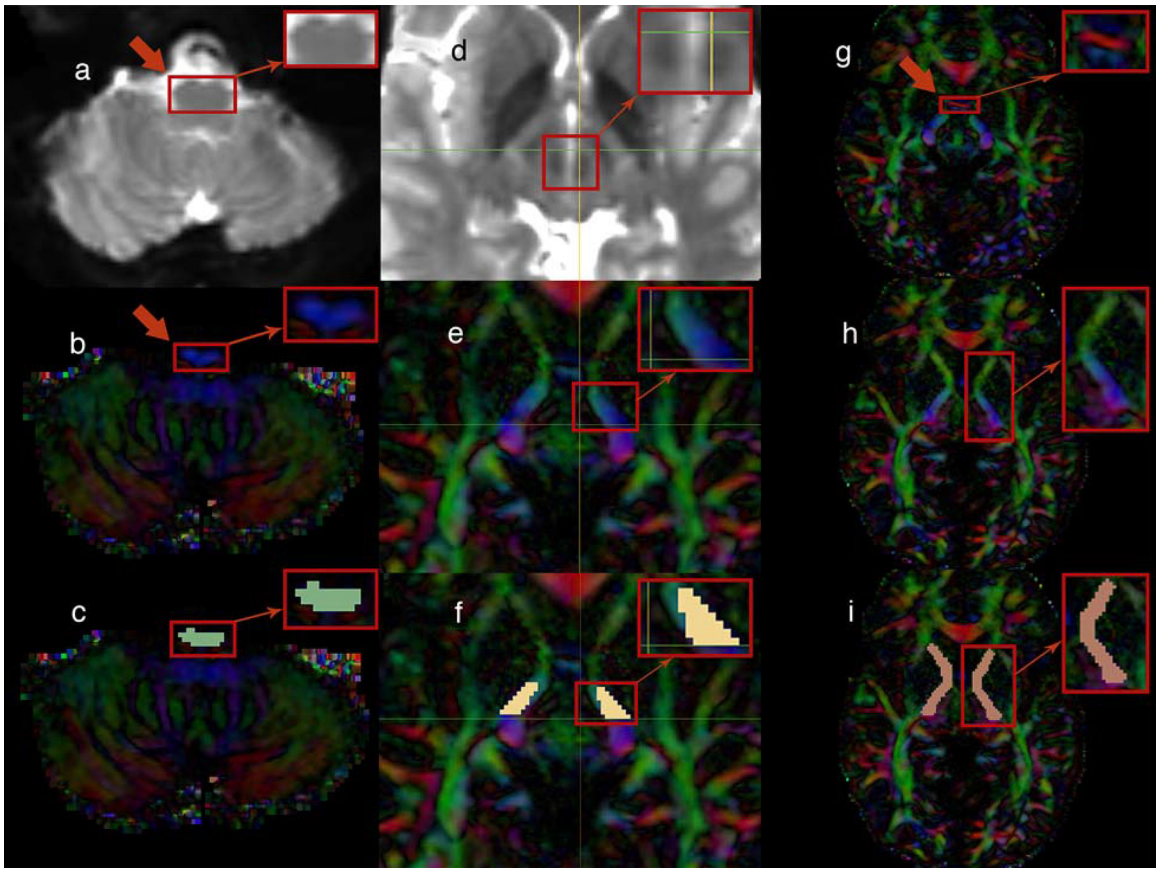

Fig. 1.

(left portion) The upper medulla oblongata, rostral to the inferior olivary nucleus, was located in the baseline (b0) MRI brain images (axial plane) as indicated by the arrow (**a**). The same area is illustrated in diffusion tensor imaging (DTI) (axial plane) as indicated by the arrow (**b**). Finally, the medulla-region-of-interest (medulla-ROI) was drawn to the targeted region (axial plane) (**c**)

(middle portion) The region included in the square was located in the baseline (b0) MRI brain images in order to detect the red nucleus (axial plane) (**d**). The region of the cerebral peduncle of the brainstem rostral to the substantia nigra and red nucleus (thereby, rostral to the horizontal level marked by the green line in the image) was targeted (axial plane) (**e**). Finally, the brainstem-ROI was drawn to that area (axial plane) (**f**)

(right portion) The anterior commissure (AC) level was located as indicated by the red color-coded fibers that disappear in the next image (axial plane) (see the red arrow) (**g**). Just after the AC was no longer visualized in the DTI and moving superiorly, the internal capsule (IC) was targeted as illustrated (axial plane) (**h**). Therefore, the capsular-ROI was drawn to the IC at the level of the AC (axial plane) (**i**)

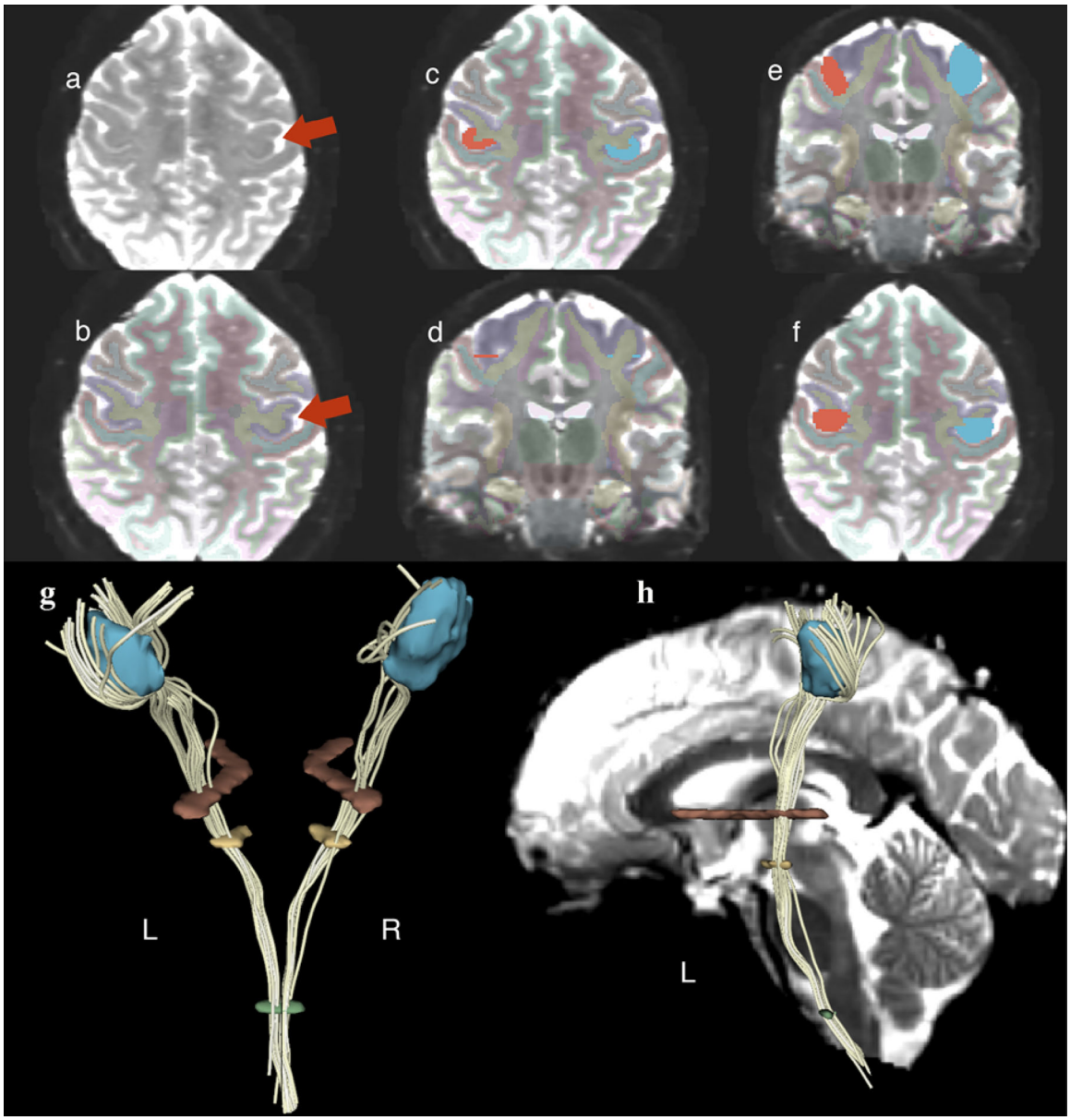

Fig 2.

(upper portion) Illustrative demonstration of the hand motor area isolation methodology using a fourth region of interest (ROI) in the precentral gyrus (cortical-ROI).

(left subsection) Detection of the "omega sign" in the precentral gyrus as indicated by the arrow (axial plane) (**a**). Confirmation of the correct localization via overlaying the FreeSurfer labelmap for each case that was a result of the automatic FreeSurfer subcortical segmentation. The purple color indicates the precentral gyrus (axial plane) (see the red arrow) (**b**).

(middle subsection) Drawing of the cortical-ROI in the cortical region of the "omega sign" (axial plane) (**c**). Detection of the same area in the coronal plane utilizing the "slice intersections" tool of 3D Slicer (coronal plane). Note that either a straight line covering the

entire extent of the gyrus of interest or two bullets defining the gyrus of interest can be observed as illustrated in the image (**d**).

(right subsection) The remaining non-colored area of the gyrus of interest was filled in with the same color to complete the cortical-ROI (coronal plane) (**e**). In the axial plane, the correct area of interest, namely the hand motor area, was verified (**f**).

(lower portion) Spatial representation of all four ROIs after they were added to one labelmap in order to isolate the hand-related motor fiber tracts (HMFTs). HMFTs were defined in White Matter Query Language (WMQL) as the fiber tracts passing through all four ROIs, as demonstrated in the case of that HMFT. Posterior view of a 3D model of the four ROIs and the HMFT passing through all four in 3D Slicer software. Left and right sides are designated L and R, respectively (**g**). Lateral view (left side) of the same subject's HMFT with an added sagittal MRI section of the subject's b0 MRI image to illustrate spatial localization of the ROIs (**h**).

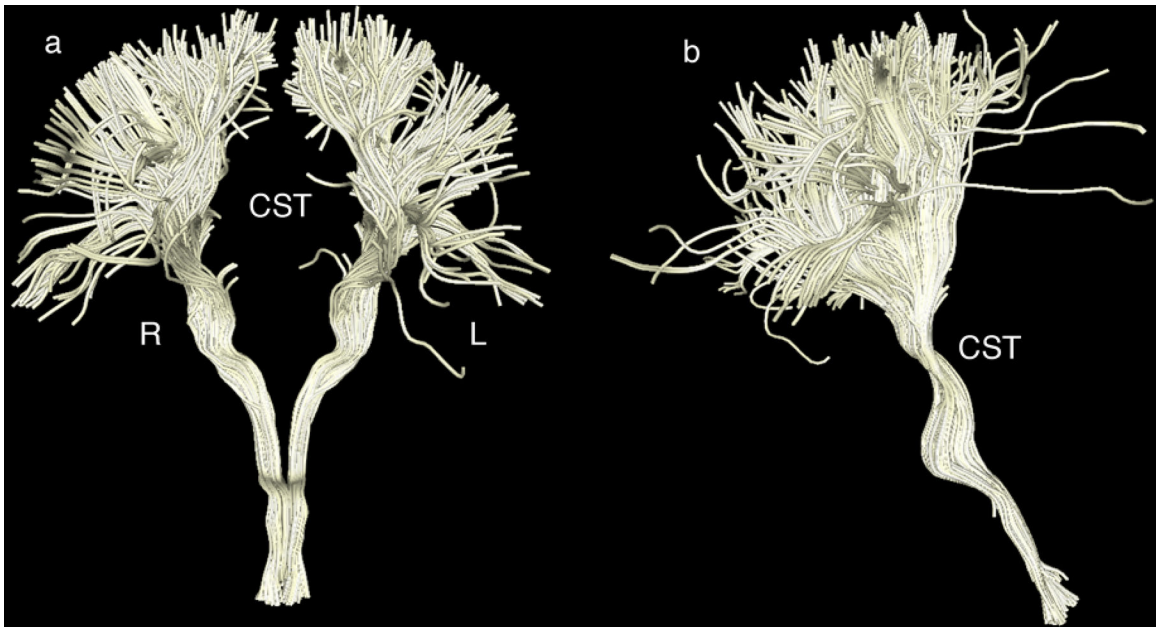

Fig. 3.

Representative corticospinal tract (CST) delineation using the three manually drawn regions of interest (ROIs) (in the medulla, brainstem and internal capsule as described in section 2.4.1) for maximum precision.

a Front view of the CST in the coronal plane. The left side is labeled L and the right side R.

b Side view (right side) of the CST (coronal plane)

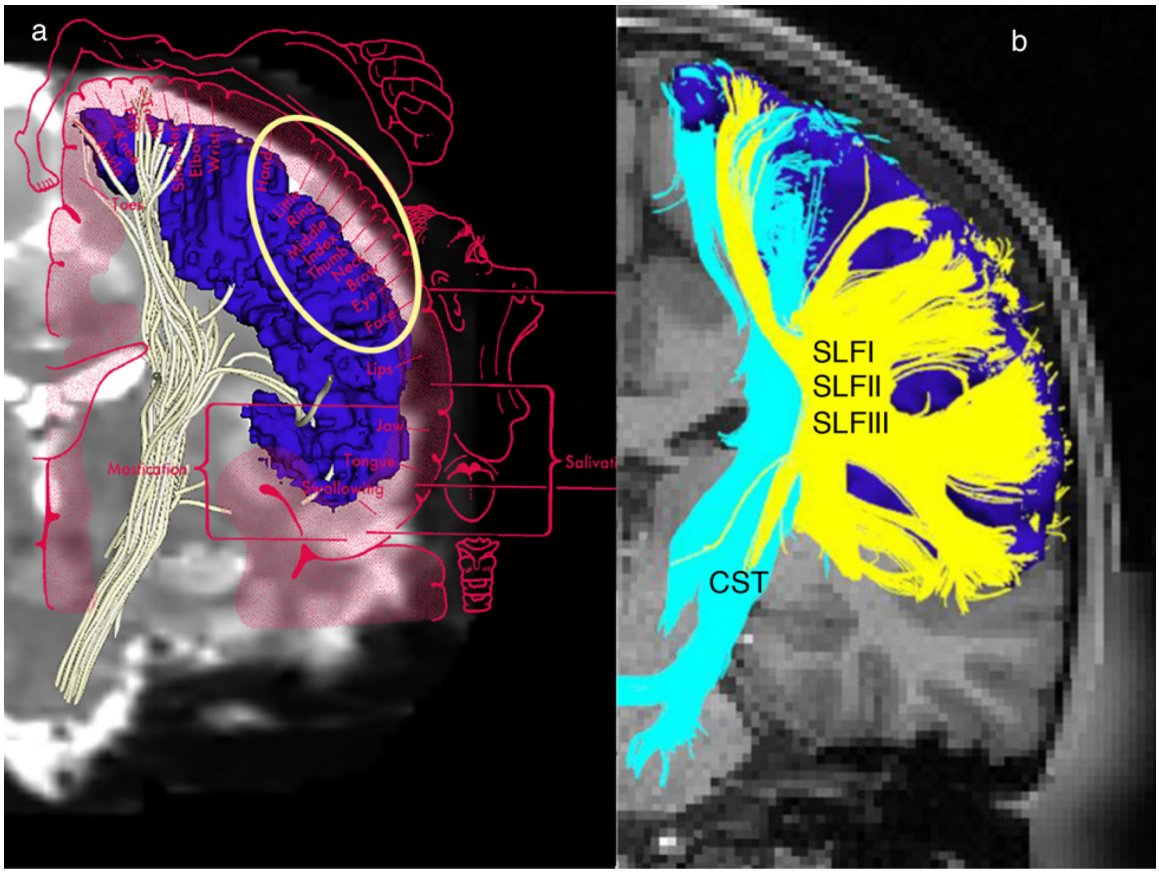

Fig. 4.

a A representative corticospinal tract (CST) of a healthy human subject delineated by diffusion magnetic resonance imaging (dMRI) tractography using high-resolution data of the Human Connectome Project (HCP) (Washington University; abbreviated as WashU) sample. Please note the paucity of fibers in the lateral aspect of the hemispheres. This is possibly due to limitations of dMRI tractography.

When overlaid with the motor homunculus (coronal plane), the lateral part of the motor homunculus indicates that the hand motor area, which should have been a part of the CST, is significantly limited, something that can possibly be explained by the presence of massive superior longitudinal fascicles I, II and III (SLF I, II and III) crossing fibers at the centrum ovale.

b In this representative case, the entire precentral cortex (dark blue) has been used as the seed to grow the CST (light blue).

Crossing fibers at the centrum ovale relating principally to the SLF I, II and III (in yellow) (Makris et al. 2005) do not allow effective sampling of CST from the lateral aspect of the precentral gyrus (motor cortex).

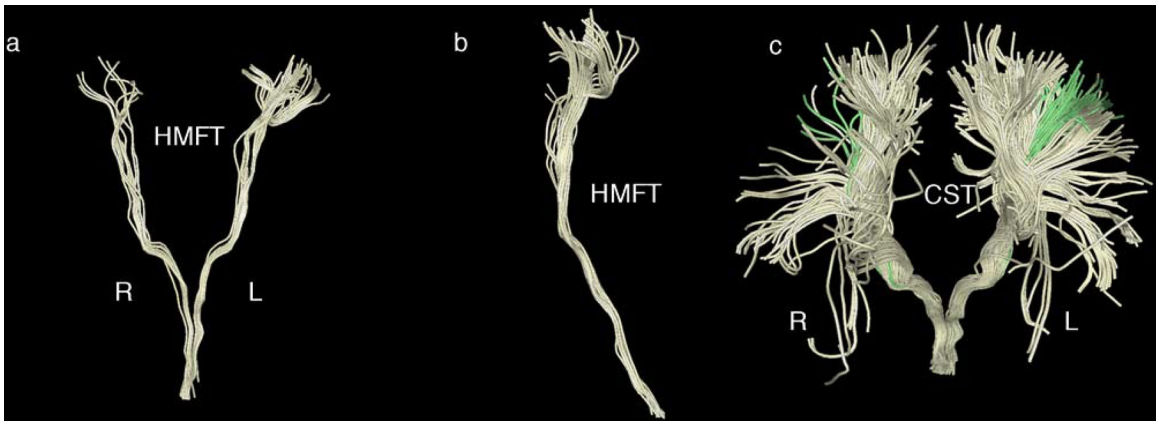

Fig. 5.

Representative hand-related motor fiber tracts (HMFTs) delineation using the four manually drawn regions of interest (ROIs) (in the medulla, brainstem, internal capsule and the "omega sign" in the precentral gyrus, as described in section 2.6) for maximum precision. It should be noted that, likely due to the current limitations of diffusion resonance imaging (dMRI) tractography, we could not obtain an optimal representation of the hand motor area in all subjects and there was significant variability among the subjects, contrary to our corticospinal tract (CST) results.

a Front view of the HMFTs in the coronal plane. The left side is labeled as L and the right as R.

b HMFTs viewed from the right side (coronal plane).

c Front view of the CST (light yellow). The HMFT (green) is depicted as a subset of the CST for direct comparison.

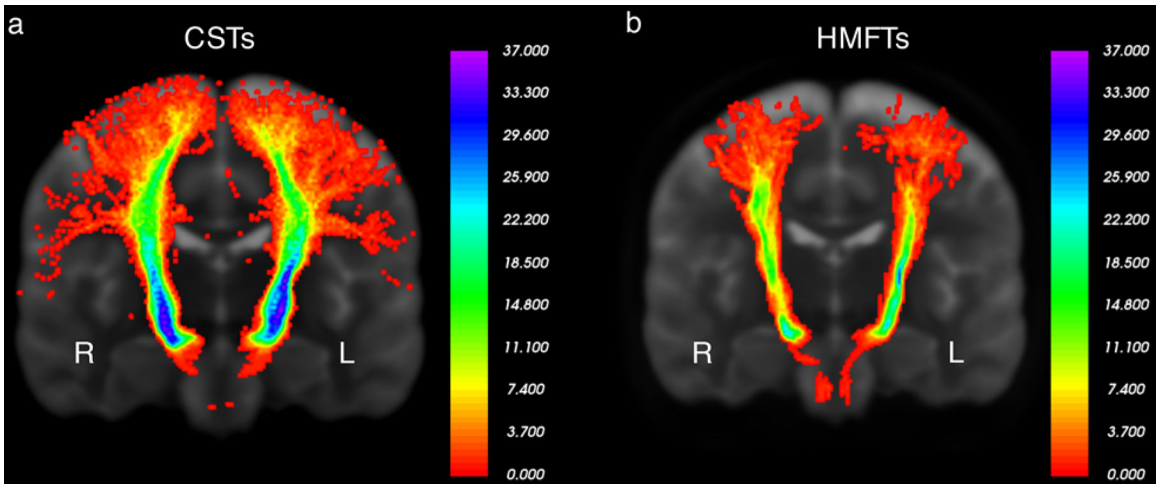

Fig. 6.

a Variability probabilistic heat map of the corticospinal tract (CST) in our 37 Washington University (WashU) healthy human subjects in the coronal plane. As indicated by the scale in the image, all or nearly all of our subjects had CST fibers passing from areas adjacent to the regions of interest (ROIs), with more variability in the cortical projections. Left is labeled as L and right as R.

b Variability probabilistic heat map of hand-related motor fiber tracts (HMFTs) in our 37 WashU healthy human subjects in the coronal plane. Left is labeled as L and right as R. Despite the use of the same methodology on state-of-the-art data, the difference in variability is noticeable, potentially indicating limitations of the current tools in diffusion tensor imaging (DTI) image analysis.

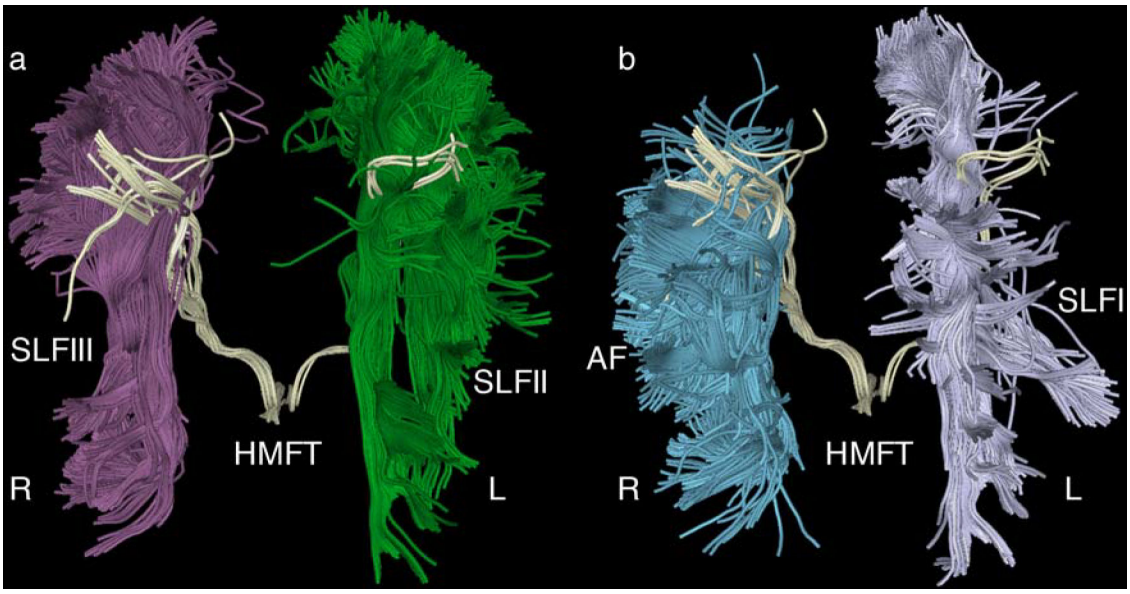

Fig. 7.

a Illustrative representation of the interference of superior longitudinal fascicle II (SLFII) (green) and SLFIII (purple) with the hand-related motor fiber tracts (HMFTs). This is an anterior view of an average case of a delineated HMFT (light yellow). SLFII and SLFIII appear to pass through the region of the corticospinal tract (CST) and, in particular, through the hand motor area. There are many “openings” within the HMFTs due to the passage of crossing fibers, which possibly affect the density of the delineated tract using diffusion magnetic resonance imaging (dMRI) tractography.

b Depiction of the SLFI (gray) on the left and the arcuate fascicle (AF) (blue) on the right. AF seems to interfere with the HMFTs laterally, whereas SLFI appears to interfere medially. The right and left sides are marked as R and L, respectively, in all figures.

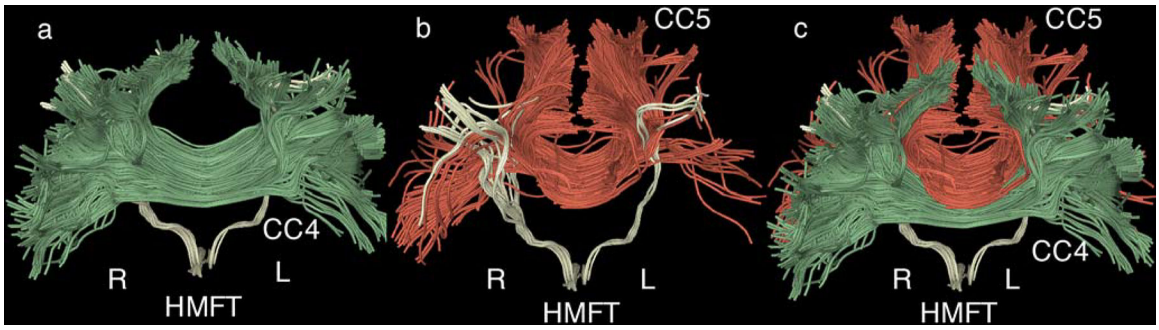

Fig. 8.

a Illustrative representation of the interference of the corpus callosum 4 (CC4, anterior midbody of the corpus callosum, in green) with the delineated hand-related motor fiber tracts (HMFTs). This is an anterior view of an average case of a delineated HMFT (light yellow). The entire HMFT seems to be affected by the crossing fibers, especially in its anterior aspect.

b Depiction of the corpus callosum 5 (CC5, posterior midbody of the CC, in red) and its spatial correlation to the HMFTs (light yellow). This is the same anterior view of the HMFT. There is less interference than observed with respect to CC4, but the HMFTs' density seems to be affected by the presence of crossing fibers in the posterior area.

c Combined anterior representation of the previously illustrated CC4 (green) and CC5 (red) to show how heavily those fibers appear to interfere with the HMFTs. All fibers are co-registered in the same Montreal Neurological Institute (MNI) 152 space. The right and left sides are marked as R and L, respectively, in all figures.

Table 1

Summary of the quantitative analysis of the biophysical characteristics and tract volumes of the delineated CSTs. Note that the coefficient of variation is very small (<10%), indicating minor variability of the results among our healthy subjects. Tract volume, by contrast, was the only parameter that was highly variable among the subjects.

	FA	RD	AD	Tract Volume (cm^3)	Normalized Tract Volume (cm^3)	Length (mm)
CST	***Mean***	***Mean***	***Mean***	***Mean***	***Mean***	***Mean***
	0.70808	285.78168	1265.76424	21.18664	0.01391	133.63757
	SD	***SD***	***SD***	***SD***	***SD***	***SD***
	0.01785	24.87915	57.36838	6.08293	0.00407	8.39159
	CV	***CV***	***CV***	***CV***	***CV***	***CV***
	0.02521	0.08706	0.04532	0.28711	0.29287	0.06279
Left CST	***Mean***	***Mean***	***Mean***	***Mean***	***Mean***	***Mean***
	0.70759	285.06082	1254.53178	11.08082	0.00725	133.52129
	SD	***SD***	***SD***	***SD***	***SD***	***SD***
	0.01750	24.19261	67.33187	3.75966	0.00235	9.41757
	CV	***CV***	***CV***	***CV***	***CV***	***CV***
	0.02474	0.08487	0.05367	0.33929	0.32454	0.07053
Right CST	***Mean***	***Mean***	***Mean***	***Mean***	***Mean***	***Mean***
	0.70504	287.09653	1264.45024	10.47865	0.00691	132.12170
	SD	***SD***	***SD***	***SD***	***SD***	***SD***
	0.02181	26.75149	58.84273	3.67042	0.00255	10.25023
	CV	***CV***	***CV***	***CV***	***CV***	***CV***
	0.03094	0.09318	0.04654	0.35028	0.36914	0.07758
SI CST	***Mean***	***Mean***	***Mean***	***Mean***	***Mean***	***Mean***
	0.00361	−0.00712	−0.00787	0.05586	0.04767	0.01054
	SD	***SD***	***SD***	***SD***	***SD***	***SD***
	−0.21919	−0.10046	0.13456	0.02402	−0.08102	−0.08467

Abbreviations used: CST: corticospinal tract, FA: fractional anisotropy, RD: radial diffusivity, AD: axial diffusivity, SD: standard deviation, CV: coefficient of variation, SI: symmetry index.

Table 2

Summary of the quantitative analysis of the biophysical characteristics and tract volumes of the delineated HMFTs. Note the increase in the coefficient of variation compared to the CST measurements. This indicates a much higher variability of the results among our healthy subjects (>10%), possibly due to the limitations of the currently available imaging tools, leading to outliers. In agreement with the CST quantitative measurements database, the tract volume was found once again to be much more variable among the subjects (coefficient of variation approximately 53%). Note that 12.7%, SD=5.7, of the CSTs analyzed refers to the hand motor area. This measurement was based on the normalized volumes of the respective tracts.

	FA	RD	AD	Tract Volume (cm^3)	Normalized Tract Volume (cm^3)	(HMFT/CST) *100 (%)	Length (mm)
HMFT	***Mean***	***Mean***	***Mean***	***Mean***	***Mean***	***Mean***	***Mean***
	0.67328	292.48218	1206.34166	2.77043	0.00183	12.71336	145.78101
	SD	***SD***	***SD***	***SD***	***SD***	***SD***	***SD***
	0.12130	40.23243	193.59313	1.38335	0.00093	5.74696	5.09166
	CV	***CV***	***CV***	***CV***	***CV***	***CV***	***CV***
	0.18017	0.13756	0.16048	0.49933	0.50588	0.45204	0.03493
Left HMFT	***Mean***	***Mean***	***Mean***	***Mean***	***Mean***	***Mean***	***Mean***
	0.60053	249.82454	1057.31801	1.25538	0.00083	10.98581	125.22519
	SD	***SD***	***SD***	***SD***	***SD***	***SD***	***SD***
	0.24648	104.96879	439.95864	1.00055	0.00066	9.04304	51.26034
	CV	***CV***	***CV***	***CV***	***CV***	***CV***	***CV***
	0.41044	0.42017	0.41611	0.79701	0.80137	0.82316	0.40935
Right HMFT	***Mean***	***Mean***	***Mean***	***Mean***	***Mean***	***Mean***	***Mean***
	0.68688	275.72408	1232.85584	1.54424	0.00103	14.47254	142.48962
	SD	***SD***	***SD***	***SD***	***SD***	***SD***	***SD***
	0.12130	53.30109	225.78500	0.88224	0.00060	7.31332	25.23457
	CV	***CV***	***CV***	***CV***	***CV***	***CV***	***CV***
	0.17660	0.19331	0.18314	0.57131	0.59003	0.50532	0.17710
SI HMFT	***Mean***	***Mean***	***Mean***	***Mean***	***Mean***	***Mean***	***Mean***
	−0.13415	−0.09856	−0.15330	−0.20636	−0.21596	−0.27392	−0.12898
	SD	***SD***	***SD***	***SD***	***SD***	***SD***	***SD***
	0.68072	0.65291	0.64341	0.12567	0.08928	0.21150	0.68046

Abbreviations used: CST: corticospinal tract, FA: fractional anisotropy, RD: radial diffusivity, AD: axial diffusivity, SD: standard deviation, CV: coefficient of variation, SI: symmetry index.